SUPPORTING INFORMATION

Comprehensive two-dimensional gas chromatography with peak tracking for screening of constituent biodegradation in petroleum UVCB substances

Andy M. Booth[1], Lisbet Sørensen[1*], Odd G. Brakstad[1], Deni Ribicic[1], Mari Creese[1], J. Samuel Arey[2], Delina Lyon[3], Aaron D. Redman[4], Alberto Martin Aparicio[3], Louise Camenzuli,[5] Neil Wang[6], Jonas Gros[7*]

[1] SINTEF Ocean, Trondheim NO-7465, Norway

[2] Oleolytics LLC, Lebanon, NJ, USA
[3] Concawe, Brussels, Belgium
[4] ExxonMobil Biomedical Sciences, Inc., Annandale, NJ, USA
[5] ExxonMobil Petroleum & Chemical B.V., Machelen, Belgium
[6] TotalEnergies, Paris, France
[7] Scientific consultant, Villars-sur-Glâne, Switzerland

*Corresponding authors:
Lisbet Sørensen, lisbet.sorensen@sintef.no
Jonas Gros, gros.jonas@gmail.com
Concawe, environment@concawe.eu

CONTENT SUMMARY: 39 pages

Page S3: Method S1 - 1D GC-FID Analysis
Page S3: Method S2 - Baseline correction
Page S4: Method S3 - Automated delineation and integration of peaks
Page S4: Method S4 - Correction of chromatograms and peak tables for analyte losses incurred by sample processing
Page S6: Method S5 - Chromatogram and peak table normalization and alignment
Page S8: Method S6 – Peak tracking
Page S9: Method S7 – Fitting of first-order DT50s to the tracked peaks
Page S10: Method S8 – Attribution of chemical identities to GC×GC–FID peaks
Page S11: Method S9 – Derivation of equation Eq. 1.
Page S14: Table S1. Properties of gas oils included in the study.
Page S15: Table S2. Average standard deviation (SD) of first dimension (RT1) and second dimension (RT2) retention times, before and after alignment, for 16 peaks across five chromatograms.
Page S16: Table S3. Methods for peak identity attribution.
Page S18: Table S4. Example DT50s found for a few identified compounds, compared with literature values.
Page S19: Table S5. Ratio of deuterated PAH peak volumes to the chrysene-d12 peak volume in absence of the evaporation step, for three replicate injections of a mixture of standards, as well as the average ratio and standard deviation of the ratio over the three replicates.
Page S19: Table S6. Overview of sample numbers and sample information.

Page S20: Figure S1. One dimensional GC-FID chromatograms of SRGO (A) and VHGO (B).
Page S21: Figure S2. Incubation system comprising 2.3 L Pyrex bottles on slowly rotating (0.75 rpm) carousels in the dark at 13 °C.
Page S21: Figure S3. Dissolved oxygen (DO) concentration in the experimental seawater containers as a function of incubation time for VHGO, SRGO, and non-oil containing controls (named “Seawater”)
Page S22: Figure S4. Median oil droplet sizes of VHGO and SRGO determined by Mulitsizer Coulter Counter (100 µm aperture) analyses of samples (triplicate) collected at regular time points during the biodegradation study
Page S23: Figure S5. Depletion in oil droplet concentration (as a percentage of the start concentration; day 0) and total extractable material (TEM) concentration quantified by 1D GC-FID (corresponding to the C10+ fraction)
Page S24: Figure S6. Region of the chromatogram selected for application of the peak-tracking algorithm (dark blue region) overlaid on an example chromatogram
Page S25: Figure S7. GC×GC–FID chromatograms at the different time points of the experiment.
Page S26: Figure S8. Remaining non-tracked C10+ mass fraction throughout the experiment for VHGO (blue) and SRGO (green) oil
Page S26: Figure S9. Tracked peaks having DT50s in the range <1-10 d (filled circles) overlaid on the day-0 chromatogram, for VHGO oil
Page S27: Figure S10. Tracked peaks having DT50s in the range 10-20 d (filled circles) overlaid on the day-0 chromatogram, for VHGO oil.
Page S27: Figure S11. Tracked peaks having DT50s in the range 20-30 d (filled circles) overlaid on the day-0 chromatogram for VHGO oil
Page S28: Figure S12. Tracked peaks having DT50s in the range 30-40 d (filled circles) overlaid on the day-0 chromatogram for VHGO oil
Page S28: Figure S13. Tracked peaks having DT50s 40-60 d (filled circles) overlaid on the day-0 chromatogram for VHGO oil.
Page S29: Figure S14. Tracked peaks having DT50s >60 d (filled circles) overlaid on the day-0 chromatogram for VHGO oil.
Page S30: Figure S15. Succession of microbial communities in the VHGO and SRGO, relative to non-oil-containing controls, over the 64 day incubation period.
Page S31: Figure S16. Chromatograms of a raw, non-weathered oil
Page S32: Figure S17. Remaining mass fraction after evaporative loss based on deuterated PAH peak ratios (open circles, Eq. 2.) and fitted exponential curve used for chromatogram and peak table correction for evaporative losses (solid lines, Eq. 1.)
Page S33: Figure S18. Conceptual depiction of the evaporation correction procedure.
Page S34: Figure S19. Set of selected alignment points overlaid on a day-0 chromatogram.
Page S35: Figure S20. Depiction of the template peaks, target peaks , and search ovals for the template peaks, overlaid on a subset of the day-0 GC×GC–FID chromatogram.
Page S36-S38: References for SI
Page S39: Excel worksheet with peak volumes (relative to day 0) of each tracked peak for each of the sampling time points

METHODS

Method S1 - 1D GC-FID Analysis

Samples (1 µL) were introduced at 330°C in pulsed splitless mode. Separation was achieved using a Zebron ZB-5MSplus column (30 m length, 0.25 µm film thickness and 0.25 mm internal diameter). The carrier gas was He at a constant flow rate of 1.0 mL/min. The column oven temperature was programmed at 40 °C (1.0 min), ramped by 6 °C/min until 325°C (10 min hold).

Method S2 - Baseline correction

Conceptually, we view that the GC×GC–FID total instrument signal consists of four categories:[1] (i) resolved analyte signal, (ii) signal attributed to unresolved material, (iii) instrument background signal (i.e., a stable, non-zero FID value in absence of sample-related material), and (iv) random fluctuations (detector noise). We assume the presence of unresolved material[1] which corresponds to a large number of small, overlapping peaks that are not chromatographically resolved, and corresponds to the two-dimensional equivalent of the "unresolved complex mixture" (UCM) often observed in one-dimensional gas chromatograms of petroleum substances.[2-7] The unresolved material is difficult to quantify and its mass fraction depends, to some extent, on the subjective choice of parameters of the baseline-correction algorithm. For quantification of individual peaks over the whole chromatogram using the GC Image automatic peak delineation and integration algorithm, baseline correction in the current study was performed with the Eilers algorithm,[1, 4, 8-11] using algorithm parameters $\lambda = 10^{4.5}$, and $p = 0.001$. This choice of parameter values[1, 4, 12] aims to remove both the instrument background signal and the unresolved material signal (Figure S16b), leaving behind the resolved analyte signal (Figure S16c).[1, 4, 13] The Eilers baseline-correction algorithm is therefore viewed as particularly appropriate for quantification of individual analytes. [1, 4, 13] We further imposed that the Eilers baseline cannot be locally lower than the estimated instrument background signal, which was calculated with the baseline algorithm of Reichenbach et al.[14] (as implemented in the GC Image software). Separately, baseline correction of the raw GC×GC–FID chromatograms was performed with the Reichenbach et al.[14] algorithm (Figure S16d) to provide chromatograms including both resolved and unresolved oil components (Figure S16e) for a few results involving the whole chromatogram mass rather than individually-tracked peaks. Taken together, the unresolved material plus resolved analyte peaks account for all of the GC×GC-amenable material that was injected into the instrument (in the present study, the C_{10+} mass was studied based on the GC×GC–FID data). The baseline correction with the algorithm of Reichenbach et al.[14] (as implemented in the GC Image software) used the following (default) parameters: default algorithm; 5 deadband data points; 7.00 for the distribution; 7 for the filter window size; and 1 stride per modulation cycle. Repeating the procedure for VHGO using a λ value of 10^5 in the Eilers algorithm led to a change ≤20% of the DT_{50} for 94% of the tracked peaks. Due to the increased mass fraction apportioned to peaks rather than to unresolved material, the mass of the day 0 oil tracked as individual peaks is increased by 4.3–4.5% when using a value of 10^5 instead of $10^{4.5}$. Consequently, this operational and subjective choice of the value of the λ parameter in the Eilers algorithm, when performed within reasonable bounds, is considered to have had a relatively small effect on the calculated DT_{50}s. Previous work suggested that a range of 10^4 to 10^5 is appropriate for quantification of individual analytes.[1]

Method S3 - Automated delineation and integration of peaks

After baseline correction, a second algorithm is needed to delineate and integrate resolved constituent peaks. This task was performed with the inverted watershed algorithm included in the GC Image software,[15] using the chromatograms baseline-corrected with the Eilers algorithm, an automatic approach previously shown to perform well in comparison with other tested approaches for peak quantification.[1] We acknowledge that any automatic peak-quantification approach may result in some level of uncertainty for a fraction of the quantified peaks due to the limitations of the automated baseline-delineation algorithm and of the automated peak-delineation algorithm. However, automated approaches are necessary to integrate the thousands of peaks present in a single chromatogram, due to the unaffordable amount of time that would be necessary to integrate them with expert manual integration or user-guided semi-automated methods. The parameters selected in the GC Image algorithm were: smoothing of 0.1 (Col. I) and 1 (Col. II); filter of 35 (minimum area), 0 (minimum volume), and 5 (minimum peak), with a "relative" minimum peak reference. For each chromatogram, this resulted in a list of peaks (*peak table*), providing first and second dimension retention times, as well as the integrated peak signal (*peak volume*), for each peak. A peak usually corresponds to one chemical constituent but can also correspond to two or more co-eluting constituents of a very similar chemical structure. The retention time of a peak is defined as the retention time for its highest signal pixel. To ensure that chromatographic regions affected by the solvent signal or those not containing oil constituents were excluded, only those peaks eluting within the range 30–215 min in the first dimension were retained for subsequent analysis, i.e. the C_{10+} constituents. To exclude the column bleed signal, peaks eluting 0.25–1.35 s before the *n*-alkanes in the second dimension were discarded. The region of the chromatogram selected for peak tracking is displayed by the dark blue region in Figure S6. For the 58 oil-containing chromatograms (42 experimental samples + 16 sterile controls), this approach resulted in the detection of 4,168–5,587 peaks. For the blank chromatograms (6 blanks containing seawater only), which contained a large number of small peaks, the 1,000 largest detected peaks in the peak tables were retained for further analysis. Any peak in the oil-containing chromatograms that had the possibility of being confounded with any of the 1,000 seawater blank peaks was considered as potentially affected by background, non-oil signal (section *Method S6*).

Method S4 - Correction of chromatograms and peak tables for analyte losses incurred by sample processing

The mixture of deuterated PAH standards (naphthalene-d_8, acenaphthene-d_{10}, fluorene-d_{10}, phenanthrene-d_{10}, and chrysene-d_{12}) was spiked into the water samples immediately before extraction to quantify evaporative losses of semi-volatile oil constituents during the sample concentration process. Because the sample concentration step relies on evaporation of the solvent, it is expected that some evaporative losses will affect the most volatile constituents of the samples during this laboratory step. Such losses are expected and varied slightly from sample to sample (Figure S17), reflecting minor variations in the processing procedure. This process decreased the concentrations of semi-volatile constituents relative to less volatile constituents, thereby affecting the constituent signal intensities that were recorded by the GC×GC–FID. Correction for evaporative losses is important for the earlier part of the chromatogram, where the peak volumes of the internal standards indicated losses of 10 to 53% of naphthalene-d_8 during the evaporation step, depending on the sample. To compensate for these evaporative losses, the GC×GC–FID data of each sample was corrected. To do this, it was assumed that the evaporative loss of each analyte in the GC×GC–FID chromatogram could be related to its first-dimension retention time, which provides a proxy of pure

liquid vapor pressure for that analyte.[16, 17] Additionally, it was expected that the extent of the evaporative loss would depend exponentially on the pure liquid vapor pressure of affected constituents, assuming a well-mixed liquid that undergoes mass transfer limited by the air boundary layer[16, 18] and consistent with previous experience.[19, 20] In other words, the fraction lost through evaporation is expected to follow an approximately exponential curve along the first dimension of each individual GC×GC–FID chromatogram with maximal loss at earliest elution times, decreasing to zero loss at the highest retention times. The corresponding equation is:

$$f_{remaining}(t_{1,i}) = e^{-k_{1,i} \cdot t_{1,i}^{-0.5} \cdot e^{-k_2 \cdot t_{1,i}}} \quad \text{(Eq. 1.)}$$

where $f_{remaining}$ is the fraction of mass remaining after the evaporation step as a function of $t_{1,i}$ the first-dimension retention time in chromatogram i, and $k_{1,i}$ and k_2 are fitted constants. The constant k_2 (one value for the complete data set sharing a single GC×GC–FID method) represents the dependence of the pure liquid vapor pressure on the first-dimension retention time, whereas the constants $k_{1,i}$ (one value per chromatogram) represents the magnitude of the exposure to evaporation. Equation 1. is derived in section *Method S9*).

With these assumptions, the peak tables and chromatogram signal data were adjusted for evaporative losses throughout the semi-volatile elution region of the GC×GC–FID chromatogram, based on the observed signal intensities of the five deuterated internal standards which spanned first dimension retention times of 47.8 min (naphthalene-d_8) to 153.8 min (chrysene-d_{12}). The evaporative loss process was expected to influence each internal standard to a different extent, according a trend that follows an exponential relationship with decreasing first dimension retention time (Eq. 1). The selected standards span the range of elution times observed to exhibit evaporative losses, and their chemical properties are very close to that of the corresponding non-deuterated PAH constituents, as demonstrated by very similar GC×GC retention times, which makes them appropriate constituents for performing the correction. As evaporative losses during sample processing can differ widely from sample to sample, each sample was adjusted individually.

The exponential curve of evaporative loss was predicted for any first-dimension retention time across the GC×GC–FID chromatogram based on the five deuterated PAHs (Figure S18a), allowing the peak volumes and chromatogram signal to be corrected for this loss (Figure S18b,c). Deuterated PAH standards were injected prior to the evaporation step at fixed relative concentrations, such that the ratio of their peak volumes to the peak volume of the less volatile of these deuterated standards (chrysene-d_{12}) would be expected to have a known value in absence of the evaporation step. The peak-volume ratio in presence of the evaporation step divided by the peak-volume ratio in absence of the evaporation provides the remaining fraction (one minus the evaporative loss) of a given deuterated standard:

$$F_{remaining,i} = \frac{\left(\frac{V_i}{V_{chrysene-d_{12}}}\right)_{with\ evaporation}}{\left(\frac{V_i}{V_{chrysene-d_{12}}}\right)_{without\ evaporation}} \quad \text{(Eq. 2.)}$$

where $F_{remaining,i}$ is the fraction of the deuterated PAH standard i remaining after the evaporation step, and V is a peak volume. The parameters $k_{1,i}$ and k_2 in Eq. 1 were fitted to the $F_{remaining,i}$ values determined through Eq. 2, and were then used to correct the peak volumes and chromatograms to

their values in the absence of evaporative losses. This correction aims to remove a potential bias resulting from the necessary sample processing steps, allowing accurate quantification of the relatively volatile constituents.

The peak volumes of the deuterated PAHs internal standards relative to the chrysene-d_{12} peak volume in a standard mixture sample unaffected by evaporation ($\left(\frac{V_i}{V_{chrysene-d_{12}}}\right)_{without\ evaporation}$) were first determined. This was based on three replicate GC×GC–FID analyses of a mixture of standards comprising a total of ~100 molecules (individual hydrocarbons such as normal alkanes and PAHs, as well as the deuterated PAH mixture), which did not include the evaporation step. Peak volumes were determined using a 2-D Gaussian curve-fit algorithm,[19] with the exception of the chrysene-d_{12} peak volume. Within the (non-evaporated) triplicate chromatograms of the standard mixture, chrysene-d_{12} coeluted with benz(a)anthracene. These two peaks were deconvoluted using an algorithm developed by Tom O'Haver.[21] Peak volume ratios for the selected deuterated PAHs to chrysene-d_{12} had standard deviations of ≤1.4% across the three replicate non-evaporated chromatograms (Table S5), which indicated excellent reproducibility (precision) of the combined analytical measurement and peak integration algorithm.

The peak volumes of the deuterated PAH internal standards (relative to the chrysene-d_{12} peak) within the samples affected by evaporation were determined using a 2-D Gaussian curve-fit algorithm. Eqs. 1 and 2 were then used to fit coefficients $k_{1,i}$ and k_2, resulting in a curve of $f_{remaining}$ for each chromatogram (Figure S17). These curves were used for the correction of evaporative losses in both the integrated peak tables and the full chromatograms (the correction corresponds to multiplying by $1/f_{remaining}$, Figure S18 and Eq. 1).

Method S5 - Chromatogram and peak table normalization and alignment

Normalization of the chromatograms was necessary to enable comparisons across chromatograms resulting from the full set of samples over the duration of the experiment. Peak volumes in GC×GC–FID chromatograms depend (a) on the concentration in the original samples (which is usually of interest to the analyst), but also (b) on the mass of extract analyzed (and on the concentration of the extract). The aim of normalization is to remove contribution (b). Therefore, to evaluate the precise changes in constituent mass between different samples, it is useful to normalize these samples using conserved marker compounds.[22, 23] In the present study, the chromatograms and peak tables were normalized to the peak volume of hexachlorobenzene, a conserved marker added to the oil prior to the degradation experiment for this purpose. Hexachlorobenzene was interpreted to be conserved, as this peak volume remained constant with respect to that of a sesquiterpene peak (tentatively identified as $C_{16}H_{30}$-8-β(H)-homodrimane) with 16.7% and 12.6% standard deviation over all of, respectively, SRGO and VHGO samples (excluding the sterile controls). A second compound that had been added to the oil as a second possible conserved marker, *o*-terphenyl, was found to be preferentially degraded relative to hexachlorobenzene (based on peak ratios) and was therefore excluded for chromatogram normalization. Peak volumes were calculated using the manually guided 2-D Gaussian curve-fit algorithm developed by Arey et al.[19] (programmed in Matlab) which enables accurate determination of individual peak volumes for well-separated peaks.[4, 19, 22] The algorithm fits a Gaussian curve plus a linear local baseline to each modulation of a peak, and then determines the modulations contributing to the peak (failure of the algorithm to determine the modulations contributing to a peak can be corrected manually).

The ratio of the total FID signal of the C_{10+} oil-containing region of the chromatograms (after the Reichenbach et al. baseline correction) to the hexachlorobenzene peak volume showed standard

deviations of 2.7 and 13.8% over 11 non-biodegraded chromatograms for each of VHGO and SRGO oil, respectively. These statistics indicate good reproducibility in the peak integration algorithm and in the approach used to account for the total oil mass (the C_{10+} oil-containing region is defined on Figure S6). Response factors of FID detectors for petroleum hydrocarbons vary by only ±10%,[24] therefore a single response factor was assumed over the whole chromatogram[4, 25] when the total chromatogram mass was calculated. Finally, simulated distillation data indicated that the distribution of boiling points within the oil largely overlapped with the range covered by the first dimension of the GC×GC–FID chromatograms: the C_{10+} mass (which was monitored with the GC×GC–FID data) represented 96.09 and 93.61% of the total substance mass for VHGO and SRGO, respectively.

The alignment algorithm developed by Gros et al.[10, 26] can be applied to each pixel of a chromatogram or to a peak table. Here, the algorithm was applied separately to chromatograms and to the retention times of peak tables. Consequently, the peak volume integration step was applied to the unaltered chromatographic signal, thereby avoiding any (small) bias resulting from interpolation during peak alignment.[10, 13, 27] The algorithm relies on so-called *alignment points*.[10] Alignment points correspond to peaks that are known or interpreted to represent the same analyte on both a reference and a target chromatogram. Alignment points were chosen among the chromatographic peaks whose position could be unambiguously attributed throughout the set of chromatograms, taking advantage of the peak patterns of oil composition to locate a peak across different chromatograms, and including some non-constituent peaks (such as internal standards). In the current study, a set of 12 alignment points was selected that encompassed the region of interest of the chromatogram.[10] The retention times of these alignment points in the aligned chromatogram (or in the aligned peak table) are made identical to their retention times in the reference chromatogram. Retention times of all other pixels in the aligned chromatogram (or peaks in the aligned peak table) are obtained by interpolation of the displacement observed for the alignment points between the target and reference chromatograms. A detailed description of the algorithm has been published,[10] and the algorithm code is publicly available.[26] To enable peak matching across the two studied oils, as well as across the different time points in the experiment, a decision was made to align all the chromatograms to a single reference chromatogram (one of the day-0 chromatograms of VHGO oil). The selected alignment points are displayed on Figure S19 (pink circles). Typical peak widths of 0.35 min and 0.2 s in the first and second dimension, respectively, were used in the algorithm.

The alignment algorithm has been shown in the past to improve retention time reproducibility across chromatograms.[10, 27] Here, we verified this outcome for the chromatographic conditions and alignment points selected for the present experiment. To achieve this aim, five procedural blanks spiked with PAHs and a few other standards were analyzed with the same method as the experimental samples, followed by alignment with the algorithm. The spiked standards enabled unambiguous identification of 16 peaks across the 5 chromatograms, which were used to verify that the alignment led to improvement in retention time correspondence across chromatograms (Table S2). The retention times of these peaks were recorded both before and after alignment. The standard deviation of the retention times for each peak across the five chromatograms was calculated and the average standard deviation across all the peaks are reported at the bottom of Table S2. This analysis confirmed the importance of the alignment step in the procedure, which decreased the average standard deviation of first dimension retention time shifts from 0.71 to 0.30 pixels (i.e., 0.083 to 0.035 min; calculated over 13 peaks, Table S2). The average standard deviation of the second-dimension retention time shifts was similarly decreased from 3.9 to 1.5 pixels (i.e., 0.039 to 0.015 s; calculated over 13 peaks, Table S2). Maximum deviations, which particularly affect the ability of the peak tracking algorithm, were also decreased by a factor of 1.9 and 2.9 for the first- and second-dimension retention times, respectively (Table S2).

Method S6 – Peak tracking

Peak tables frequently contain thousands of integrated chromatographic peaks. Once the algorithms described above have been applied to these peak tables, it is of particular interest to identify how peaks corresponding to a given constituent change over the course of the experiment (days 0 to 64), in order to infer biodegradation rate constants or DT_{50}s. However, the large number (thousands) of peaks separated by GC×GC–FID means that automated peak tracking algorithms are needed to track the hundreds or thousands of constituent peaks across chromatograms.[10, 22, 28] Here we use a new algorithm, which is an adapted version of that reported by Wardlaw et al.,[22] such that it enables disappearance of peaks during the experiment (interpreted as losses due to biodegradation), and the new algorithm was applied to series of >2 chromatograms. In a first step, peak lists are compared two by two, with one of the two always being a chosen reference peak list. This step is repeated 20 times for each oil (21 peak lists in total). In a second step, peaks that can be matched in all of the 21 peak lists are retained, using the reference peak list to identify commonly matched peaks.

One peak list was arbitrarily designated as the "template", and the other as the "target". For each peak in the peak list of the template chromatogram, a search oval was centered on the 1st and 2nd dimension peak retention time (Figure S20). If any other peak(s) within the peak list of the template chromatogram lay within the search oval radius of a given peak, then these peaks (the given peak and other peak(s)) were considered confounding and all of them were eliminated from the analysis. This happened for 363–586 peaks for VHGO oil. The search oval dimensions were chosen as 0.15 min in the first dimension and 0.075 s in the second dimension, based on the observed peak shifts in the chromatograms. If the peak was not eliminated at this step, the search oval was placed onto the target chromatogram at the same coordinates as the candidate peak of the template chromatogram. The closest peak in the peak list of the target chromatogram, if it lay within the search oval in the target chromatogram, was considered a tentative match with the (template) peak that originated the search oval. If no peak was found within the search oval in the target chromatogram, then the peak was considered a potentially successful match and labeled as "absent peak". Absent peaks are only allowed in chromatograms at ≥3 d, but these peaks must be present in all peak lists for replicate samples at day 0 (not biodegraded). If a peak in the target chromatogram peak list was closest to more than one peak in the template chromatogram peak list and if those lay within the search oval of that peak, then all of the relevant peaks (in both template and target peak lists) were rejected from the matched peaks, owing to the inability to perform an unambiguous peak matching. This happened for 197–394 peaks for any of the pairwise matchings for VHGO oil. Finally, the assignments of the template and target chromatograms were swapped, and the search procedure described above was repeated. Peaks were considered successfully matched if they were accepted by the match criteria both before and after the swap. Peaks that were present within the three day 0 chromatograms for one of the oils but found to be absent in some or all of the subsequent chromatograms with no other peaks within the search oval, were considered absent peaks (lost due to biodegradation) and assigned a mass of half the effective detection limit of the method (TMAL). In total, 3106 and 3283 peaks were matched across the three day 0 chromatograms among the 3783 and 3910 peaks ≥10*TMAL in the day 0 reference chromatogram for VHGO and SRGO oil, respectively.

The peak matching was performed on chromatograms two-by-two, with one of them always being a day 0 chromatogram for the VHGO and SRGO oils. This resulted initially in 2×20 sets of matched peaks for the biodegradation experiment (for each of the two oils) together with 6 sets of matched peaks for the blank chromatograms. For the VHGO oil, these sets of matched peaks contained 3320–3524 peaks. In a second step, each of the 20 sets of matched peaks from the biodegradation experiment were combined such as to enforce two rules: (1) a peak must be present in each of the three replicate chromatograms at day 0 to be considered a successful match, and (2) the peak must be matched across

the 21 chromatograms for a given oil (but can be considered an absent peak in any of the chromatograms at ≥3 d into the experiment). Peaks corresponding to internal standards and conserved marker molecules (added to the oil or to the extracts for the purpose of the experiment) were removed from the matched peaks in order to exclude these added chemicals from subsequent analysis. Additionally, a few of the large *n*-alkanes peaks were found to be overloaded, such that their position was shifted in the template chromatogram with respect to more biodegraded chromatograms (in which these peaks had decreased in size). This led to failure of the peak-tracking algorithm for these peaks and, consequently, the *n*-alkane peaks were manually tracked. The 1,000 largest detected peaks in the peak tables of the blank chromatograms (containing seawater only) were also tracked. Peaks that were found to be present in the 6 blank chromatograms and whose peak volumes were ≥1% of the corresponding peak in the reference (day 0) chromatogram were removed from further consideration in order to avoid bias arising from non-constituent peaks.

Finally, those tracked peaks having estimated DT_{50}s ≥40 d, which additionally had either a small size relative to local baseline and/or a high level of noise, were removed from consideration. When a peak is small relative to a locally raised baseline, its peak volume is potentially poorly determined by an approach such as the inversed watershed algorithm used here, which sums all pixels determined to belong to the peak. The DT_{50} of such a peak would risk being driven largely by the DT_{50} of the local baseline (unresolved mass remaining after application of the selected baseline-correction algorithm) rather than by the DT_{50} of the corresponding constituent. Therefore, the peak apex value was stipulated to be at least three times the local baseline. The local baseline was defined as the minimum pixel value within a window twice the size of a typical peak, centered on the peak. Additionally, some peaks exhibited high root mean squared deviations (RMSDs) relative to the fitted exponential decay curve. These peaks were suspected to be affected by non-constituent material and were removed from further consideration. As these artifacts will disproportionally affect peaks with longer DT_{50}s, these two criteria were only applied to those peaks having DT_{50}s ≥40 d.

Method S7 – Fitting of first-order DT_{50}s to the tracked peaks

After identifying peaks that could be automatically tracked over the 2×21 chromatograms, the average peak volumes across the three replicates per time point were calculated. Here, DT_{50}s were estimated by fitting exponential decay curves according to equation 3:

$$m(t) = m_0 \cdot e^{-\lambda_1 \cdot t} \qquad \text{(Eq. 3.)}$$

where m is the compound mass (peak volume) at time t, m_0 is the initial compound mass (peak volume) at the onset of the experiment, and λ_1 is the biodegradation rate constant. The values m_0 and λ_1 were determined for each peak tracked over the set of chromatograms (day 0 to day 64) such as to minimize the root-mean-squared-deviation (RMSD) between Eq. 3 and the corresponding seven average peak volumes, separately for each of VHGO and SRGO oils. At each time point, for each peak, the average peak volume of the three replicates was used. In the case of a peak being absent in some (or all) replicates, the volume of the peak in those chromatograms was counted as 0.5*TMAL. TMAL, the *tracked mass abundance limit* corresponds the smallest peak in each peak table, interpreted as the limit of detection of the approach. To ensure that the results are primarily driven by data above TMAL and only marginally sensitive to the assumption made for absent peaks, only those peaks present at day 0 at ≥10*TMAL(day 64) were retained in this study. DT_{50}s are given by:

$$t_{1/2} = \frac{ln(2)}{\lambda_1}$$

(Eq. 4.)

where $t_{1/2}$ is the DT_{50}. DT_{50}s are defined as positive for compounds exhibiting losses over the course of the experiment. For the few compounds exhibiting (principally small) mass gains over the experiment, "negative DT_{50}s" (i.e. time for mass doubling) were obtained through equation 4 (negative λ_1 values). These peaks, as well as peaks having DT_{50}s >64 d, were considered as conserved peaks and reported as having DT_{50}s ">64 d". Owing to the temporal resolution of the sampling during the experiment, it was similarly considered that the shortest resolvable DT_{50} was 1 d, and any shorter DT_{50} obtained through Equation 4 is reported as "<1 d". Using the average of the three replicates at each time step, the procedure is considered to provide the best estimate of the DT_{50}s for the tracked peaks. 68% confidence intervals of the DT_{50}s were derived with a parametric bootstrap (using 10,000 draws), assuming a Gaussian distribution of the three replicates at each time point, and using the percentile bootstrap method.[29, 30]

Method S8 – Attribution of chemical identities to GC×GC–FID peaks

Identifying the chemical compound corresponding to a given GC×GC–FID peak is an important but often difficult task. Two frequently used approaches are the injection of chemical standards to verify retention position[2, 31, 32], and the interfacing of the GC×GC instrument with a mass spectrometer (MS).[33] Inherently, an MS detector has advantages for peak identity attribution, whereas an FID detector has advantages for quantitation of peaks/compounds that lack calibration standards due to similar response factors for many classes of hydrocarbons. Finally, the repeating nature of GC×GC elution position across a chemical constituent family[2, 34] and knowledge of the constituent families expected in petroleum mixtures offers help in identifying the position of individual constituents and constituent families in chromatograms.

Use of chemical standards for peak identification. Chemical standards (sometimes as mixtures of standards) can be injected on the GC×GC–FID instrument, where comparison of retention times allows peak identification in the GC×GC–FID chromatogram of samples.[2] This approach leads to robust peak identity assignments for well-separated peaks, such as non-substituted PAHs and deuterated PAHs. Another approach is to analyze a sample twice on the GC×GC–FID instrument, once without and once with added chemical standards. In this approach, the position of the chemical standard peak is identified by the change of the peak magnitude between the two chromatograms. This second approach may be more appropriate for regions of chromatograms where a large number of constituents elute in close proximity, owing to the potential of retention time shifts between two different chromatograms.[35] Chemical identity attribution through the use of chemical standards is prone to potential misidentifications in the case where two different chemicals would coelute. Qualitatively, this risk is higher in peak-dense regions of the chromatograms and smaller to negligible for well-separated peaks with predictable retention patterns, such as parent PAHs and normal alkanes. The risk of misidentification of individual constituent peaks usually increases with the degree of alkylation, due to two factors, i) increased number of isomers and ii) co-elution with other constituents of similar retention properties.

Use of mass spectrometry for peak identification. MS enables the chemical structure of a peak to be evaluated. For peak identification, the use of an MS is superior to the use of an FID as the actual structure of the material constituting the peak is investigated. However, peak identification with a MS

is also prone to misidentifications or failed identifications. The potential sources of such failures include an inability to determine the corresponding peak positions in the GC×GC–FID and GC×GC–MS chromatograms and identification difficulties when common diagnostic ions are shared by several chemical classes. As above, the risk of peak misidentifications is higher in peak-dense regions of the chromatograms.

Approach used in the current study for attribution of chemical identities to GC×GC–FID peaks. In the current study, chemical identities were attributed to individual peaks based on chemical standards. The mixture of standards used contained: phenol-d_6, *p*-cresol-d_8, naphthalene-d_8, 4-*n*-propylphenol-d_{12}, acenaphthene-d_{10}, fluorene-d_{10}, phenanthrene-d_{10}, 5α-androstane, chrysene-d_{12}, perylene-d_{12}, naphthalene, acenaphthene, fluorene, phenanthrene, chrysene, perylene, phenol, *o*-cresol, *p*-cresol, benzothiophene, 2,4-dimethylphenol, 2,4,6-trimethylphenol, 4-isopropylphenol, 3,5-dimethylphenol, 4-ethylphenol, 4-tert-butylphenol, 2,3,5-trimethylphenol, decalin, decahydro-1-methylnaphthalene, 2,6-dimethylnaphthalene, 2,3-dimethylnaphthalene, 4-*n*-butylphenol, 4-*n*-pentylphenol, 4-tert-butyl-2-methylphenol, 2-tert-butyl-4-methylphenol, 4-isopropyl-3-methylphenol, 2,3,5-trimethylnaphthalene, 1,2,5,6-tetramethylnaphthalene, dibenzofurane, biphenyl, dibenzothiophene, anthracene, acenaphthylene, 4-methyldibenzothiophene, 1-methylphenanthrene, *o*-terphenyl, 1-methylfluorene, fluoranthene, 1,2-dimethylphenanthrene, 3,6-dimethylphenanthrene, 2,6,9-trimethylphenanthrene, 1,2,6,9-tetramethylphenanthrene, 1-methylpyrene, benzo(a)anthracene, 1-methylchrysene, benzo(b) fluoranthene, benzo(k)fluoranthene, pyrene, benzo(a)pyrene, dibenzo(a,b)anthracene, indeno(1,2,3-c,d)pyrene, benzo(g,h,i)perylene, 17α(H),21β(H)-hopane, C_{10}–C_{40} *n*-alkanes, pristane, and phytane.

The only exception was the sesquiterpene peak, which we describe as 'tentatively identified as $C_{16}H_{30}$-8-β(H)-homodrimane', which was tentatively identified based on retention time comparison with previous studies and discussion with a GC×GC–FID expert not directly involved in the current study. Chemical family elution regions were identified either purely based on previous studies or based on a mix of information from previous studies and the use of a small number of chemical standards belonging to those families (see list of standards used above). For each peak identity attribution performed in the current study, Table S3 shows the method used for this peak identity attribution, a qualitative description of the risk of misidentification and of the risk of the additional presence of constituents differing from the attributed identity, and the part of the article where these identifications are cited.

Method S9 – Derivation of equation Eq. 1.

In this section, we derive equation 1, which expresses evaporative losses of constituents due to sample handling in the laboratory. Eq. 1 relates the extent of evaporative loss to the first-dimension retention time in a GC×GC–FID chromatogram, where the first-dimension retention time represents a proxy for constituent volatility from a nonpolar phase. When exposed to a gas phase devoid of constituent *i*, the evaporative flux is given by:[18]

$$F_{i,s/a} = -v_{i,s/a} \cdot C_{i,s} \qquad \text{(Eq. 5.)}$$

where F is a flux (kg s^{-1} m^{-2}), *v* is a mass transfer coefficient or mass transfer velocity (m s^{-1}), and *C* is a concentration (kg m^{-3}); *a* denotes the gas phase, *s* the liquid solvent phase, and *s/a* the movement

from phase *s* to phase *a*. Based on the magnitudes of the thermodynamic solvent-air partition constants of the affected semi-volatile constituents (e.g., naphthalene), the limitation to mass transfer is assumed to lie in the gas phase, and the mass transfer velocity is:[25]

$$v_{i,s/a} = v_{i,a} \cdot K_{i,a/s} \qquad \text{(Eq. 6.)}$$

where $v_{i,a}$ is the mass transfer velocity across the gas-phase boundary layer, and $K_{i,a/s}$ is the (unitless) gas-solvent partition coefficient.

Therefore:

$$F_{i,s/a} = -v_{i,a} \cdot K_{i,a/s} \cdot C_{i,s} \qquad \text{(Eq. 7.)}$$

where:[18]

$$K_{i,a/s} = \frac{\gamma_{i,s} \cdot \overline{V_s}}{R \cdot T} \cdot p^*_{i,L} \qquad \text{(Eq. 8.)}$$

where $\gamma_{i,s}$ is the activity coefficient of constituent *i* in the solvent, $\overline{V_s}$ is the molecular volume of the solvent, *R* is the gas constant, *T* is the temperature, and $p^*_{i,L}$ is the sub-cooled liquid vapor pressure of constituent *i*. The activity coefficient, $\gamma_{i,s}$, is assumed equal to 1 for hydrocarbon constituents in a nonpolar solvent. The term $\frac{\gamma_{i,s} \cdot \overline{V_s}}{R \cdot T}$ is approximately constant for a given laboratory setting and will thereafter be called C_1.

Based on the equation for the mass flux given by Eq. 7, and taking consideration of Eq. 8, the mass change of constituent *i* through evaporation (during the solvent evaporation step), $\left.\frac{dM_i}{dt}\right|_{evap}$, is:

$$\left.\frac{dM_i}{dt}\right|_{evap} = -v_{i,a} \cdot C_1 \cdot p^*_{i,L} \cdot C_{i,s} \cdot A \qquad \text{(Eq. 9.)}$$

where *A* is the surface area of the interface (assumed constant for a given laboratory setting).

Because the concentration of constituent *i* in the solvent is the ratio of the mass of constituent *i* by the volume of solvent $\left(C_{i,s} = \frac{M_i}{V_s}\right)$, this implies that:

$$\int_{M_0}^{M(\tau)} \frac{1}{M_i} dM_i = \int_0^{\tau} -v_{i,a} \cdot C_1 \cdot p^*_{i,L} \cdot \frac{A}{V_s} dt \qquad \text{(Eq. 10.)}$$

where τ is an effective evaporation time. Integrating equation 10 gives:

$$ln\left(\frac{M(\tau)}{M_0}\right) = -v_{i,a} \cdot C_1 \cdot p^*_{i,L} \cdot \frac{A}{V_s} \cdot \tau \qquad \text{(Eq. 11.)}$$

when assuming that V_s is constant. From Eq. 11, we further interpret that:

$$f_{remaining}(t_{1,i}) = \frac{M(\tau)}{M_0} = e^{-v_{i,a} \cdot C_1 \cdot p^*_{i,L} \cdot \frac{A}{V_s} \cdot \tau} \qquad \text{(Eq. 12.)}$$

where $t_{1,i}$ is the first-dimension retention time in a GC×GC–FID chromatogram.

It has been shown that there is a linear relationship between $ln(p^*_{i,L})$ and $t_{1,i}$.[17] Moreover, empirical correlations indicate that $v_{i,a}$ is approximately proportional to the molar mass to the power α, with α a coefficient ranging from -1/4 to -2/3,[1, 18] and the molar mass is approximately linearly dependent on $t_{1,i}$;[19] we assume here that α = -0.5.

Lumping all the constant terms into two coefficients, we therefore obtain:

$$f_{remaining}(t_{1,i}) = e^{-k_{1,chr} \cdot (t_{1,i})^{-0.5} \cdot e^{-k_2 \cdot t_{1,i}}} \qquad \text{(Eq. 13.)}$$

where k_2 is a constant expressing the dependency of the vapor pressure on t_1, and $k_{1,chr}$ is a constant depending in part on the evaporative exposure (through τ). Eq. 13 is equivalent to Eq. 1. Consequently, for a chosen GC×GC method, a single value of the constant k_2 applies across all generated chromatograms, whereas the constant $k_{1,chr}$ is specific to a given chromatogram, because the evaporative exposure (during the solvent volume reduction step in the laboratory) varied from sample to sample. The values of these constants were fitted to peak volumes of the deuterated standards as explained in section *Method S4*.

TABLES

Table S1. Properties of gas oils included in the study.

Test oil "ID"	SRGO	VHGO
SINTEF-ID	**2020-506**	**2020-507**
Substance name	Distillates (petroleum), full-range straight-run middle	Fuels, Diesel
CAS	68814-87-9	68334-30-5
EC	272-341-5	269-822-7
Density (g cm^{-3})	0.835	0.842
Spiked concentration hexachlorobenzene	0.732 mg/mL	0.729 mg/mL
Spiked concentration *o*-terphenyl	0.1890 mg/mL	0.2015 mg/mL

Table S2. Average standard deviation (SD) of first dimension (RT1) and second dimension (RT2) retention times, before and after alignment, for 16 peaks across five chromatograms.[a]

Compound name	Average RT1 after alignment (min)	SD of RT1 before alignment (pixels)[d]	SD of RT1 after alignment (pixels)[d]	Average RT2 after alignment (s)	SD of RT2 before alignment (pixels)[e]	SD of RT2 after alignment (pixels)[e]	Comment
phenol-d_6	26.59	0.0	0.4	1.40	2.83	2.35	
p-cresol-d_8	36.31	0.4	0.1	1.67	3.05	1.79	
naphthalene-d_8	47.93	0.5	0.4	2.08	3.58	1.50	
naphthalene	48.26	0.5	0.2	2.13	3.85	1.89	
4-*n*-propylphenol-d_{12}	56.56	0.5	0.1	1.70	2.83	1.16	
acenaphthene-d_{10}	79.10	0.8	0.0	2.64	3.65	0.00	alignment point
acenaphthene	79.64	0.5	0.5	2.67	3.39	0.51	
fluorene-d_{10}	88.64	0.8	0.0	2.73	3.65	0.97	
fluorene	89.10	0.8	0.0	2.76	3.56	0.82	
phenanthrene-d_{10}	105.57	0.5	0.5	3.50	3.63	2.38	
phenanthrene	105.92	0.5	0.5	3.52	3.21	2.18	
5α-androstane	126.92	0.9	0.4	1.71	1.92	2.01	
chrysene-d_{12}	154.00	0.9	0.0	5.13	4.72	0.00	alignment point
chrysene	154.41	1.0	0.6	5.18	5.17	0.81	
perylene-d_{12}	177.80	1.1	0.0	6.77	6.58	0.00	alignment point
perylene	178.15	1.1	0.0	6.83	7.01	1.19	
average (16 peaks)[b]		**0.71**	**0.25**		**3.9**	**1.2**	
average (13 peaks)[c]			**0.30**			**1.5**	
maximum (16 peaks)		**1.1**	**0.58**		**7.0**	**2.4**	

[a] These chromatograms were five procedural blanks (ultrapure deionized water) spiked with a set of PAHs (and a few other) compounds as well as surrogate and recovery standards. These five blank chromatograms spiked with standards enabled unambiguous identification of individual compound peaks.

[b] phenol-d_6, *p*-cresol-d_8, naphthalene-d_8, naphthalene, 4-*n*-propylphenol-d_{12}, acenaphthene-d_{10}, acenaphthene, fluorene-d_{10}, fluorene, phenanthrene-d_{10}, phenanthrene, 5α-androstane, chrysene-d_{12}, chrysene, perylene-d_{12}, perylene. The three underlined compounds were used among the selected 12 alignment points, and were therefore perfectly aligned by the algorithm (a separate, conservative statistic was consequently calculated for the 13 other peaks, i.e. when excluding these 3 peaks).

[c] Excluding acenaphthene-d_{10}, chrysene-d_{12}, and perylene-d_{12}, which were selected as alignment points (and therefore perfectly aligned by the algorithm).

[d] 1 pixel is the interval between two consecutive data points; 1 pixel in the first dimension equals 0.117 min at the selected modulation period of 7 s.

[e] 1 pixel is the interval between two consecutive data points; 1 pixel in the second dimension equals 0.01 s at the selected sampling rate of 100 Hz.

Table S3. Methods for peak identity attribution.

Compound name	Method for identity attribution	Qualitative misidentification risk for the individual peak or peak group within the VHGO and SRGO GC×GC–FID chromatograms	Qualitative risk of presence of other constituents within the peak or peak group for the VHGO and SRGO GC×GC–FID chromatograms	Text location where the peak is mentioned	Peak type
phenol-d_6	A,B[1]	very low	very low	main text, Table S5	added chemical
p-cresol-d_8	A,B[1]	very low	very low	main text, Table S5	added chemical
naphthalene-d_8	A,B[1]	very low	very low	main text, Method S4, Tables S3, S5, Figure 2	added chemical
naphthalene	A[1]	very low	very low	Method S4, Tables S2, S5, Figures 2, S9	constituent
4-*n*-propylphenol-d_{12}	A,B[1]	very low	very low	main text, Table S5	added chemical
acenaphthene-d_{10}	A,B[1]	very low	very low	main text, Method S4, Tables S3, S5	added chemical
acenaphthene	A[1]	very low	very low	Tables S2, S5, Figure S9	constituent
fluorene-d_{10}	A,B[1]	very low	very low	main text, Method S4, Tables S3, S5	added chemical
fluorene	A[1]	very low	very low	Tables S2, S5	constituent
phenanthrene-d_{10}	A,B[1]	very low	very low	main text, Method S4, Tables S3, S5	added chemical
phenanthrene	A[1]	very low	very low	Tables S2, S5, Figure S9	constituent
5α-androstane	A,B[1]	very low	moderate	main text, Table S5	added chemical
chrysene-d_{12}	A,B[1]	very low	very low	main text, Method S4, Tables S3, S5	added chemical
chrysene	A[1]	very low	very low	Table S5	constituent
perylene-d_{12}	A,B[1]	very low	very low	main text, Table S5	added chemical
hexachlorobenzene	A,B[1]	very low	moderate	main text, Method S5, Table S1	added chemical
o-terphenyl	A,B[1]	very low	moderate	main text, Method S5, Table S1	added chemical
normal alkanes	A[1,3]	very low	moderate[2]	Table S2, Figures 2, S9	constituent
pristane	A[1]	very low	very low	Table S2, Figure S9	constituent
phytane	A[1]	very low	very low	Table S2, Figure S10	constituent
1-methylphenanthrene	A[1]	low	low	Figure S9	constituent

2,3,5-trimethylnaphthalene	A[1]	low	low	Figure S9	constituent
2,6-dimethylnaphthalene	A[1]	low	low	Figure S9	constituent
2,3-dimethynaphthalene	A[1]	low	low	Figure S9	constituent
sesquiterpene peak tentatively identified as $C_{16}H_{30}$-8-β(H)-homodrimane	C[1]	moderate to high	moderate	Method S5	constituent
C_1-naphtalenes[4]	A,C[1]	very low	low	Figures 2, S9	group of constituents
C_2-naphthalenes[4]	A,C[1]	very low	low	Figures 2, S9	group of constituents
methyl-branched alkanes[4]	C[1]	low	moderate	main text, Figures 2, S9	group of constituents
alkylcyclopentanes and alkylcyclohexanes[4]	C[1]	low to moderate	high	main text, Figure 2	group of constituents
one-ring aromatics[4]	A,C[1]	low	high	main text, Figures 2, 3	group of constituents
two-ring aromatics[4]	A,C[1]	low	moderate to high	main text, Figures 2, 3	group of constituents
three-ring aromatics[4]	A,C[1]	low	moderate to high	main text, Figure 3	group of constituents
four-ring aromatics[4]	A,C[1]	low	moderate to high	main text, Figure 3	group of constituents
saturated hydrocarbons[4]	A,C[1]	low	high	main text, Figures 2,3	group of constituents

[1] The following methods were used:
A: Comparison of peak retention time with retention time in a GC×GC–FID chromatogram of a mixture of standards.
B: Peak identification with two GC×GC–FID chromatograms of (1) the petroleum substance and (2) the petroleum substance spiked with a standard of the chemical compound (this was repeated for both VHGO and SRGO).
C: Peak identification based on comparison with retention times in GC×GC–FID chromatograms of previous studies[4, 36] involving petroleum substances.

[2] Normal alkane peaks, especially when somehow overloaded in day-0 chromatograms might overlap with neighboring peaks, however the normal alkane peaks are expected to be one to several orders of magnitude larger than potentially coeluting peaks at day 0.

[3] Normal alkanes form a regular series of large peaks[e.g.,36] that are extremely easily identified in day-0 chromatograms by an experienced analyst, and the correct carbon numbers can be attributed to these peaks based on the elution positions of the phytane and pristane peaks, which were confirmed by the use of chemical standards.

[4] Groups of constituents from a given chemical family are usually relatively likely to include also some constituents from other chemical families, however the risk of misidentification of the overall region of the chromatogram for each group of constituents is usually relatively low (for petroleum substances).

Table S4. Example DT_{50}s found for a few identified compounds, compared with literature values.

Compound name	1st dimension retention time in sample 1 (min)	2nd dimension retention time in sample 1 (s)	DT_{50} for VHGO experiment (d), with 68% confidence interval in parenthesis	DT_{50} for SRGO experiment (d), with 68% confidence interval in parenthesis	Observed DT_{50} according to a database of literature values for varied conditions of salinity (freshwater/saltwater) and temperature (Supporting Information of Prosser et al., 2016[37])
naphthalene	48.18	2.11	5.3 (4.9–5.7)	—	2.1–9.6
phenanthrene	105.93	3.52	5.8 (5.5–6.1)	4.4 (3.9–5.0)	2.6–16.5
acenaphthene	79.57	2.70	14 (12.4–15.6)	—	2.5–11.6
fluorene	89.13	2.76	6.8 (6.7–7.0)	—	—
n-C_{10}	30.92	0.41	3.0 (2.8–3.2)	1.5 (1.2–1.8)	2.0–3.2
n-C_{11}	42.23	0.49	3.2 (3.0–3.3)	1.9 (1.5–2.2)	2.1–4.4
n-C_{12}	53.78	0.55	3.2 (3.0–3.4)	2.3 (2.0–2.6)	1.9–5.1
n-C_{13}	64.98	0.59	1.6 (1.5–1.7)	2.5 (2.2–2.8)	2.3–4.7
n-C_{14}	75.60	0.63	2.1 (1.9–2.2)	2.7 (2.4–2.9)	2.3–4.7
n-C_{15}	85.63	0.66	3.2 (3.1–3.3)	2.7 (2.5–2.9)	2.4–5.1
n-C_{16}	95.08	0.66	3.3 (3.1–3.5)	2.7 (2.5–2.9)	2.5–4.8
n-C_{17}	104.18	0.68	3.3 (3.3–3.4)	2.8 (2.6–3.0)	1.9–7.0
n-C_{18}	112.70	0.71	3.6 (3.4–3.7)	2.8 (2.6–3.0)	2.5–6.7
n-C_{19}	120.87	0.70	3.9 (3.8–4.0)	2.9 (2.6–3.1)	2.8–5.1
n-C_{20}	128.57	0.74	2.7 (2.5–2.8)	2.9 (2.7–3.1)	3.1–5.3
n-C_{21}	135.92	0.74	3.7 (3.6–3.9)	2.9 (2.7–3.1)	3.0–19.4
n-C_{22}	143.03	0.76	4.8 (4.5–5.1)	2.9 (2.7–3.0)	3.0–21.0
n-C_{23}	149.92	0.77	7.9 (7.1–8.9)	2.9 (2.8–3.1)	3.2–39.6
n-C_{24}	156.33	0.79	5.1 (4.4–5.9)	3.1 (2.9–3.3)	3.5–54.3
n-C_{25}	162.63	0.81	6.3 (5.6–7.1)	3.0 (2.8–3.2)	4.4–52.1
n-C_{26}	168.70	0.83	5.8 (5.2–6.5)	3.2 (2.9–3.4)	5.2–50.0
pristane	105	0.57	9.7 (9.1–10.4)	6.6 (6.2–7.0)	4.3–21.0
phytane	113.8	0.59	16.4 (15.2–17.7)	—	6.2–28.0

Table S5. Ratio of deuterated PAH peak volumes to the chrysene-d_{12} peak volume in absence of the evaporation step, for three replicate injections of a mixture of standards, as well as the average ratio and standard deviation of the ratio over the three replicates.

		Ratio of peak volume to chrysene-d_{12} peak volume, $\left(\frac{V_i}{V_{chrysene-d_{12}}}\right)_{without\ evaporation}$				
Compound name	Spiked amount (µg/sample)	Replicate 1	Replicate 2	Replicate 3	Average[a]	Standard deviation
naphthalene-d_8	2.522	6.33	6.38	6.42	**6.38**	**0.7%**
acenaphthene-d_{10}	1.000	2.39	2.42	2.43	**2.41**	**0.8%**
fluorene-d_{10}	1.000	2.23	2.27	2.29	**2.26**	**1.4%**
phenanthrene-d_{10}	0.480	1.03	1.04	1.05	**1.04**	**0.9%**
chrysene-d_{12}	0.500	–	–	–	–	–

[a] the average ratio was used in eq. 2 and for correction of evaporative loss.

Table S6. Overview of sample numbers and sample information.

Sample #	Sampling day	Sample Info
1	0	VHGO
2		
3		
4		SRGO
5		
6		
7	3	VHGO
8		
9		
10		SRGO
11		
12		
13	7	VHGO
14		
15		
16		SRGO
17		
18		
19		VHGO Sterile
20		
21		SRGO Sterile
22		
23	14	VHGO
24		
25		
26		SRGO
27		
28		
29		VHGO Sterile
30		
31		SRGO Sterile
32		

Sample #	Sampling day	Sample Info
33	21	VHGO
34		
35		
36		SRGO
37		
38		
39	28	VHGO
40		
41		
42		SRGO
43		
44		
45		VHGO Sterile
46		
47		SRGO Sterile
48		
49	64	VHGO
50		
51		
52		SRGO
53		
54		
55		VHGO Sterile
56		
57		SRGO Sterile
58		
59	0	Blank Control
60	3	Blank Control
61	7	Blank Control
62	14	Blank Control
63	21	Blank Control
64	28	Blank Control
65	64	Blank Control

FIGURES

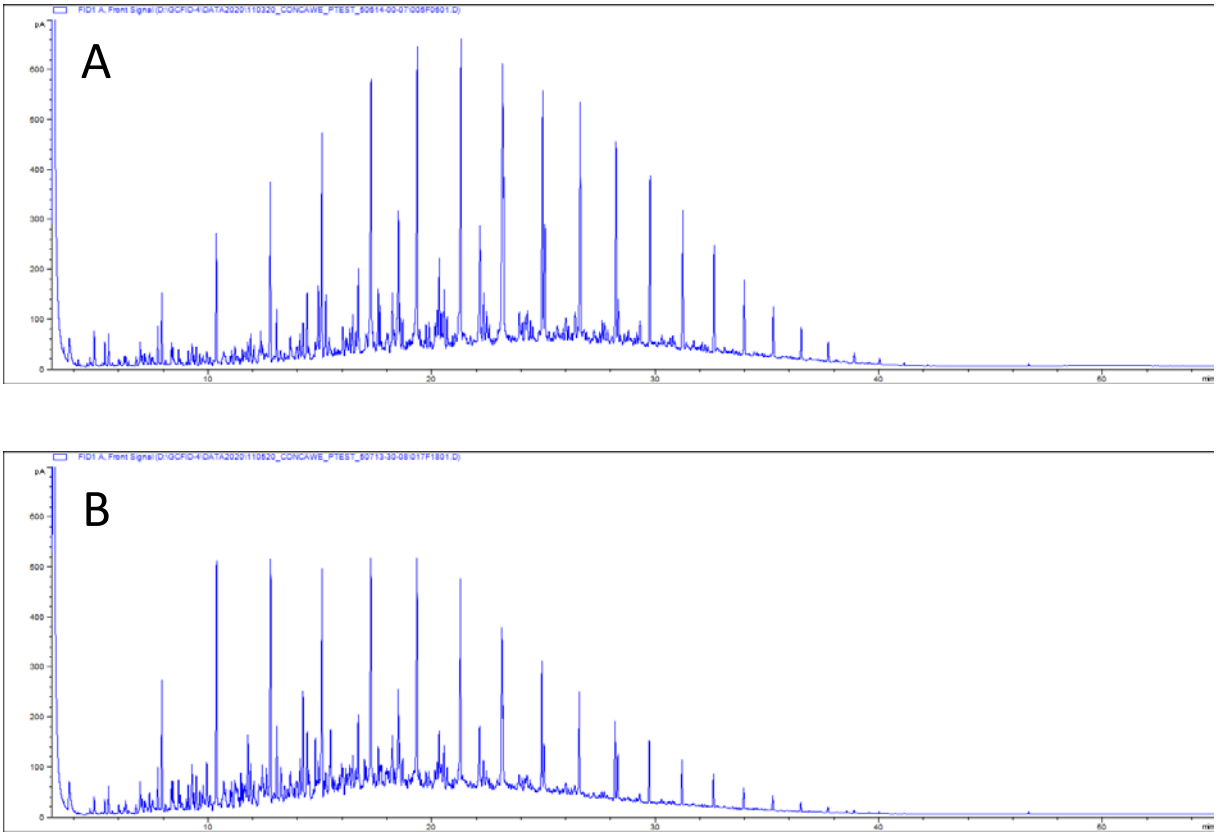

Figure S1. One dimensional GC-FID chromatograms of SRGO (A) and VHGO (B).

Figure S2. Incubation system comprising 2.3 L Pyrex bottles on slowly rotating (0.75 rpm) carousels in the dark at 13 °C.

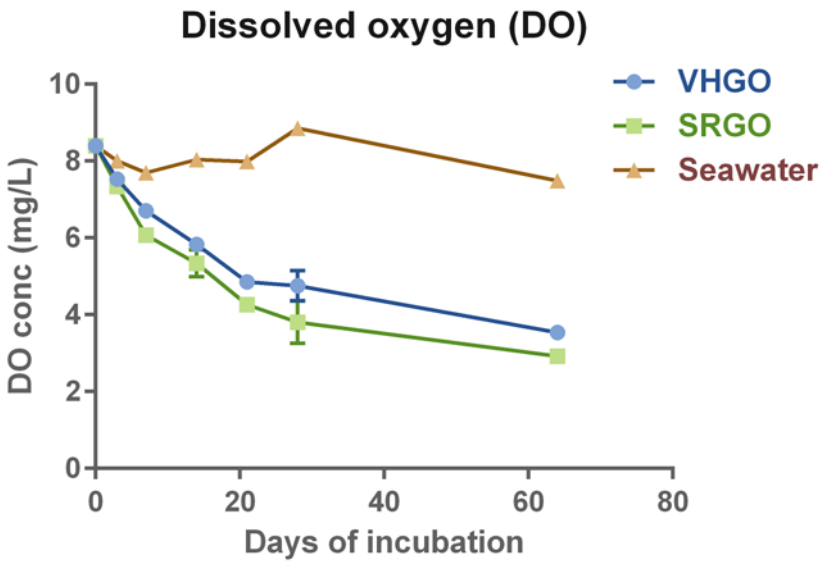

Figure S3. Dissolved oxygen (DO) concentration in the experimental seawater containers as a function of incubation time for VHGO, SRGO, and non-oil containing controls (named "Seawater"). The measured oxygen concentrations are sufficient to sustain aerobic metabolic pathways (i.e., the seawater never became oxygen-deficient, where oxygen-deficient seawater is defined as oxygen concentrations below ~3% of saturation value or ~0.3 mg L^{-1})[38]. We note that complete biodegradation of hydrocarbons to H_2O and CO_2 is expected to decrease (and not increase) the partial pressure of dissolved gases.

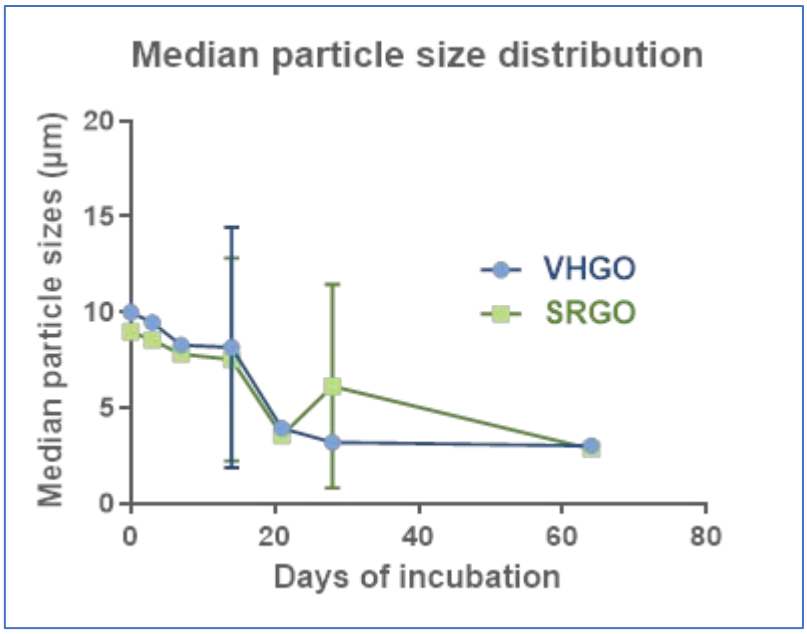

Figure S4. Median oil droplet sizes of VHGO and SRGO determined by Mulitsizer Coulter Counter (100 µm aperture) analyses of samples (triplicate) collected at regular time points during the biodegradation study.

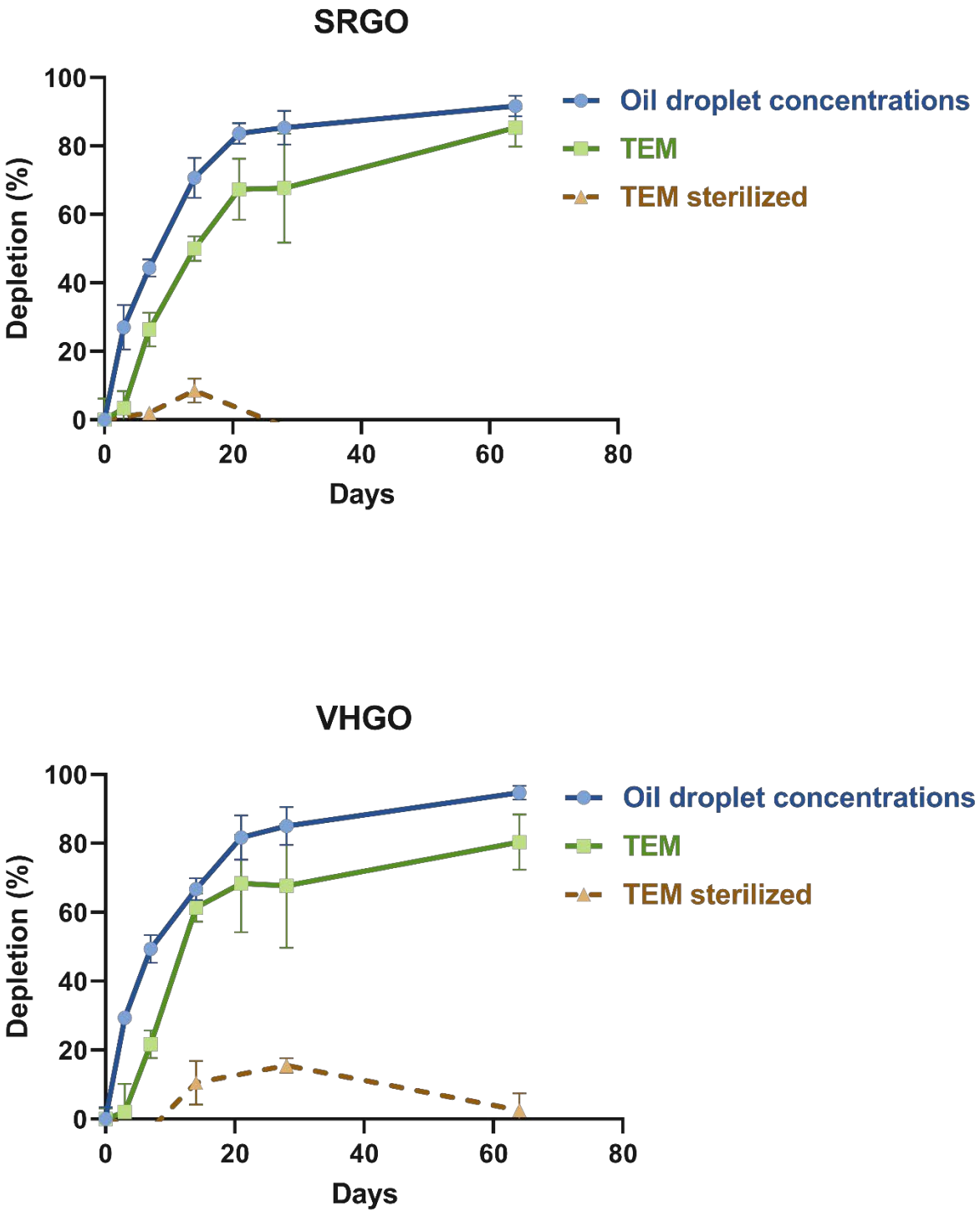

Figure S5. Depletion in oil droplet concentration (as a percentage of the start concentration; day 0) and total extractable material (TEM) concentration quantified by 1D GC-FID (corresponding to the C_{10+} fraction). TEM analyses are shown in systems with normal non-amended SW and in SW sterilized by filtration (0.2 µm filters) with added biocide (100 mg/L $HgCl_2$).

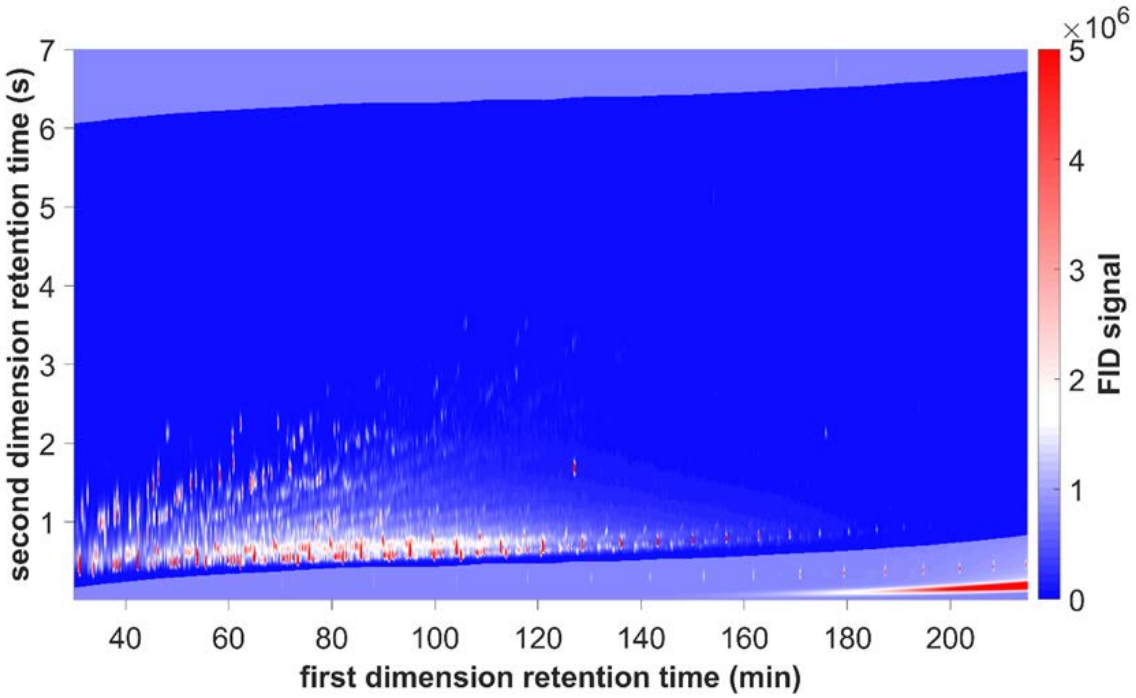

Figure S6. Region of the chromatogram selected for application of the peak-tracking algorithm (dark blue region) overlaid on an example chromatogram; this region corresponds to the C_{10+} fraction of the substances. The excluded region (lighter shades) contains peaks not corresponding to oil constituents and background interferences from column bleed.

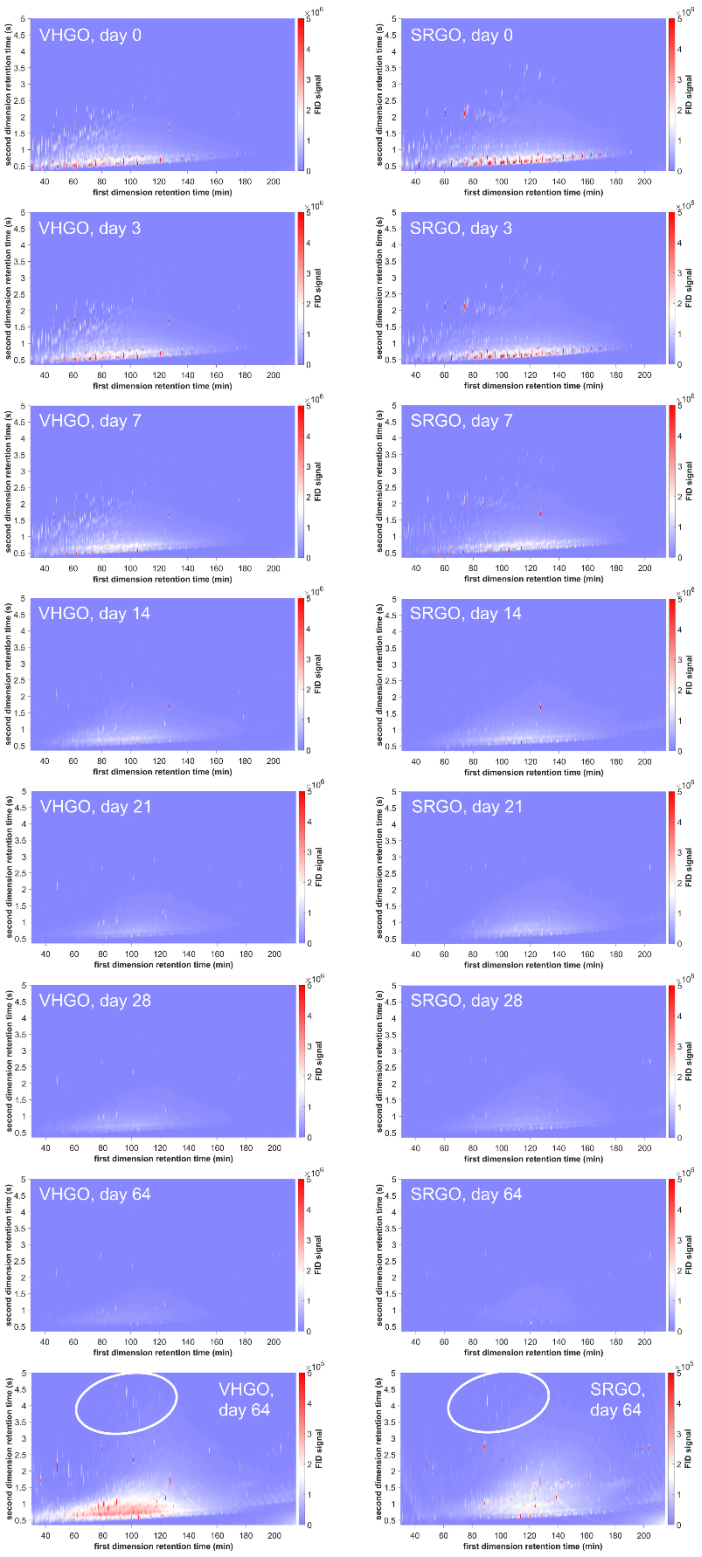

Figure S7. GC×GC–FID chromatograms at the different time points of the experiment. The chromatograms were baseline-corrected with the Reichenbach et al.[14] algorithm (Method S2), corrected for analyte losses incurred by sample processing (Method S4), normalized (Method S5), aligned (Method S5), and averaged over the three chromatograms of the three replicate samples. The two last rows show the chromatograms for day 64 with two different color axes (the last row uses a 10× magnified color axis compared to all other rows in order to highlight the peaks having low peak heights; the white ovals indicate an example of polar peaks which are putative

degradation products. These highlighted peaks appeared chiefly between days 7 and 14, corresponding to the period of most intense degradation of aromatic hydrocarbon constituents). Note: here and throughout the manuscript, the color scale uses 64 bins and peaks having peak heights lower than 1/64 times the maximum value on the color axis are invisible (on the current figure, pixels smaller than $7.8 \cdot 10^4$ are invisible as the same color is used for pixels in the range 0–$7.8 \cdot 10^4$ for rows one to seven of the figure (pixels smaller than $7.8 \cdot 10^3$ are invisible for the last row of the figure).)

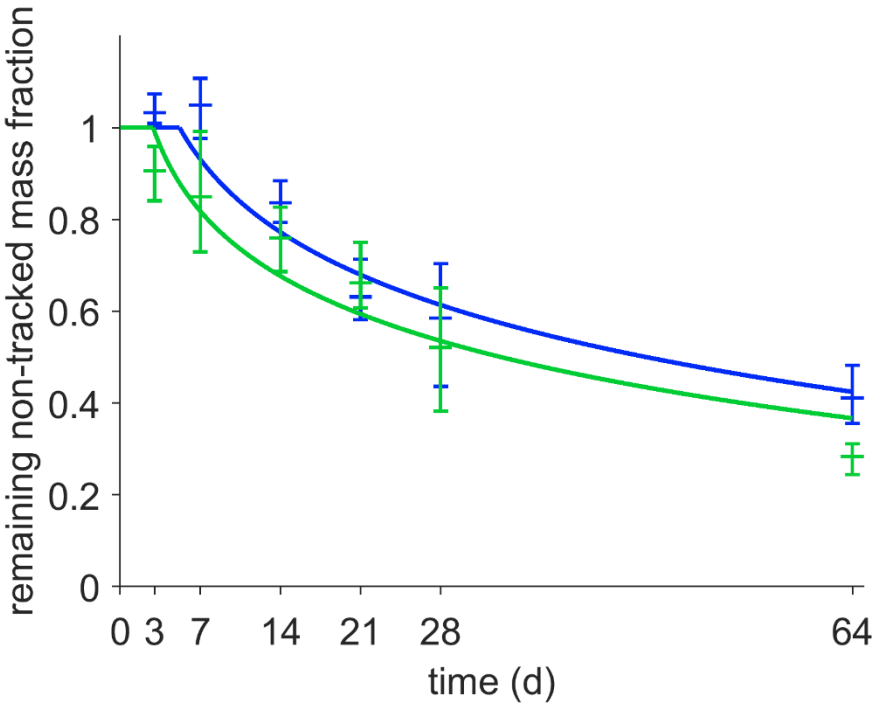

Figure S8. Remaining non-tracked C_{10+} mass fraction throughout the experiment for VHGO (blue) and SRGO (green) oil. The non-tracked C_{10+} mass was calculated as the difference between the total C_{10+} mass (determined by GC×GC-FID, Figures 1 and S6) and the sum of the peak volumes of the tracked peaks. The symbols are averages of three replicates at each time point (middle horizontal bar) and the range of the three replicates (outer horizontal bars), and the lines are fitted logarithmic decay curves with lag time.

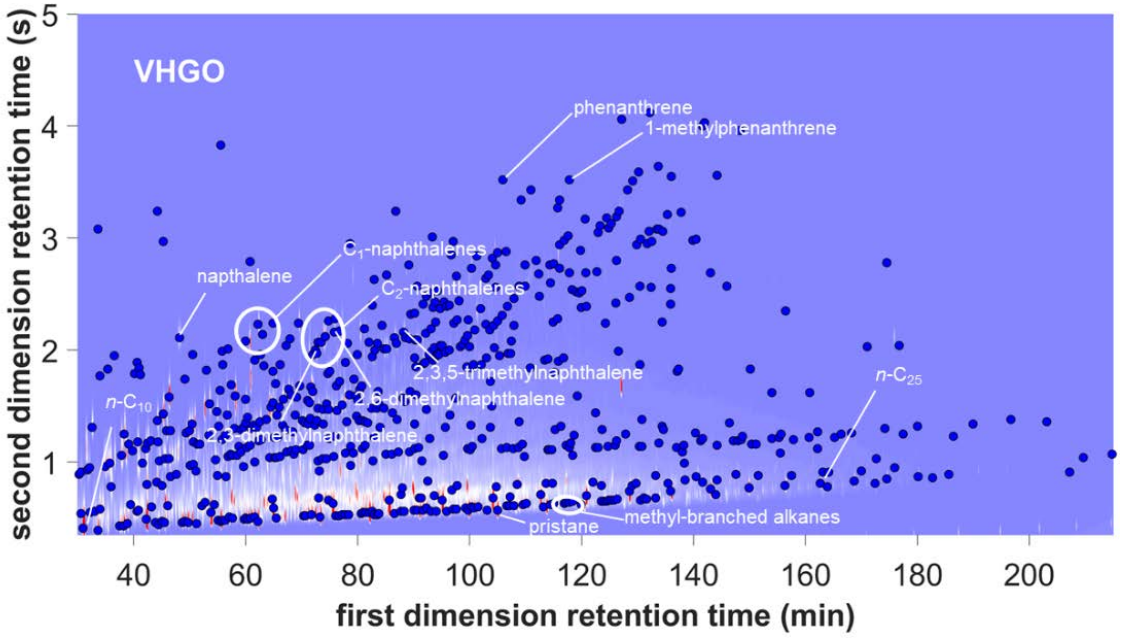

Figure S9. Tracked peaks having DT_{50}s in the range <1-10 d (filled circles) overlaid on the day-0 chromatogram, for VHGO oil. Compound labeling is based on analysis of a mixture of standards.

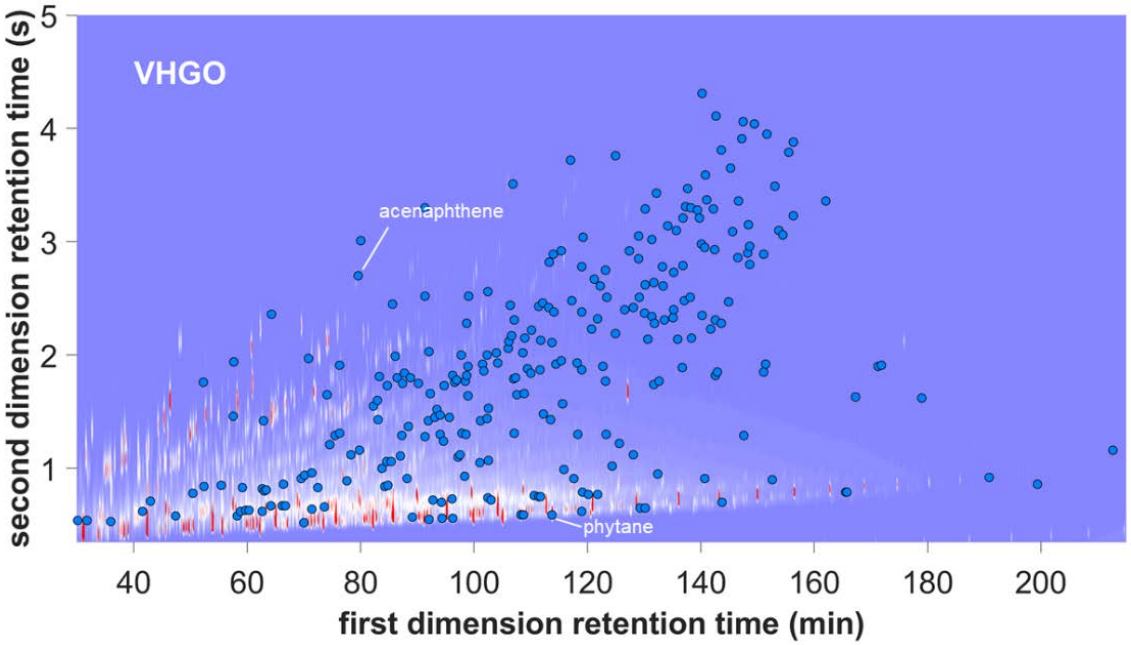

Figure S10. Tracked peaks having DT_{50}s in the range 10-20 d (filled circles) overlaid on the day-0 chromatogram, for VHGO oil. Compound labeling is based on analysis of a mixture of standards.

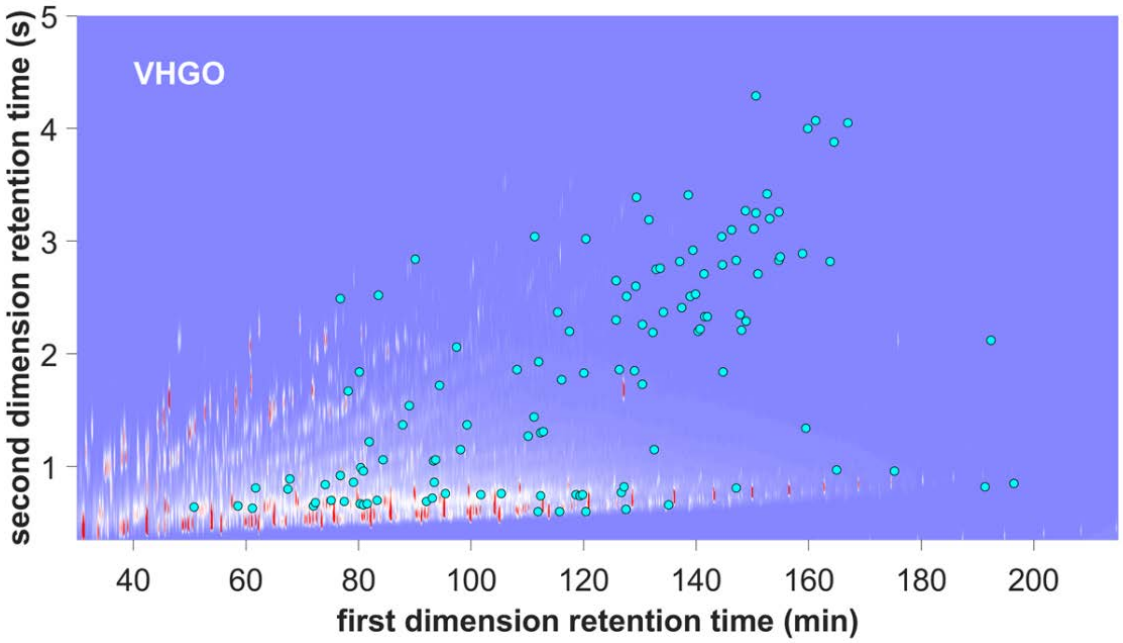

Figure S11. Tracked peaks having DT_{50}s in the range 20-30 d (filled circles) overlaid on the day-0 chromatogram for VHGO oil.

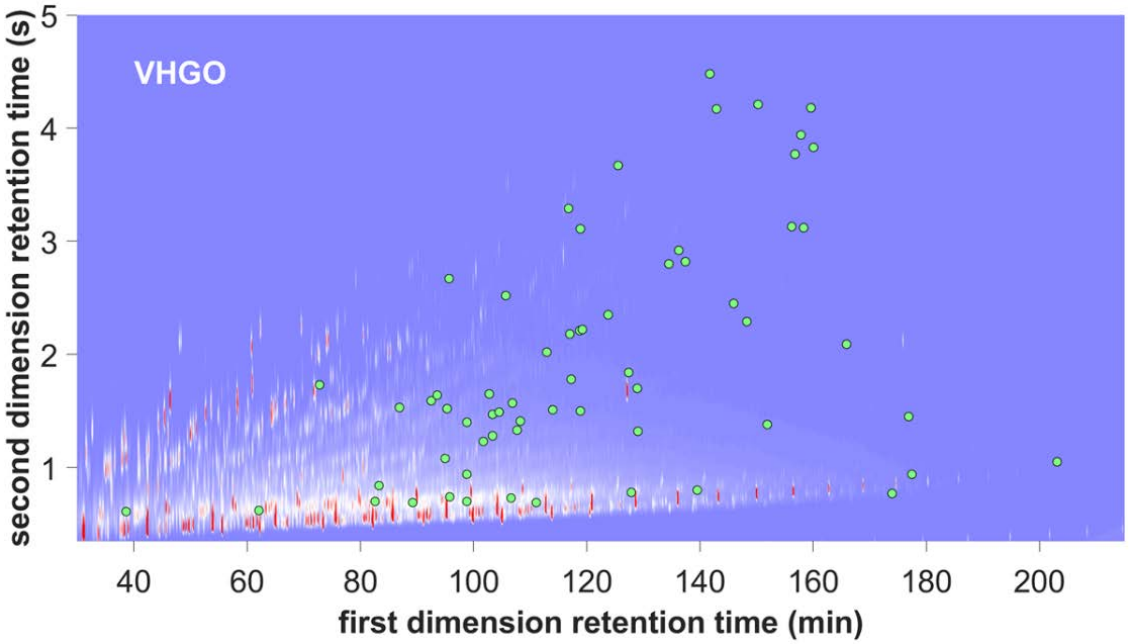

Figure S12. Tracked peaks having DT_{50}s in the range 30-40 d (filled circles) overlaid on the day-0 chromatogram for VHGO oil.

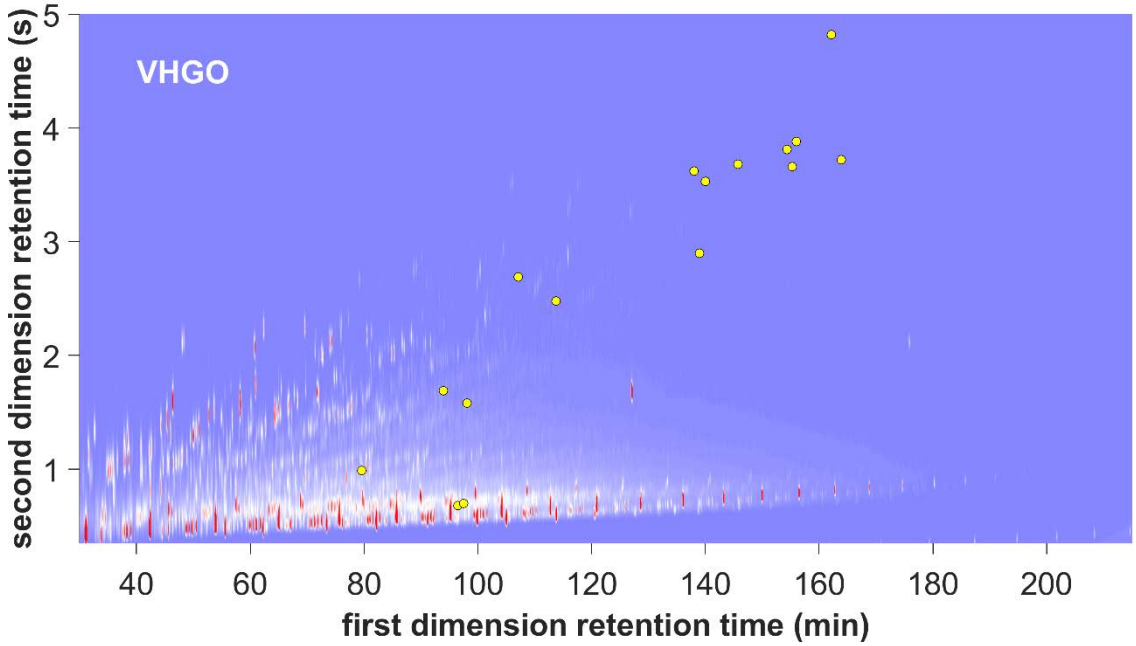

Figure S13. Tracked peaks having DT_{50}s 40-60 d (filled circles) overlaid on the day-0 chromatogram for VHGO oil.

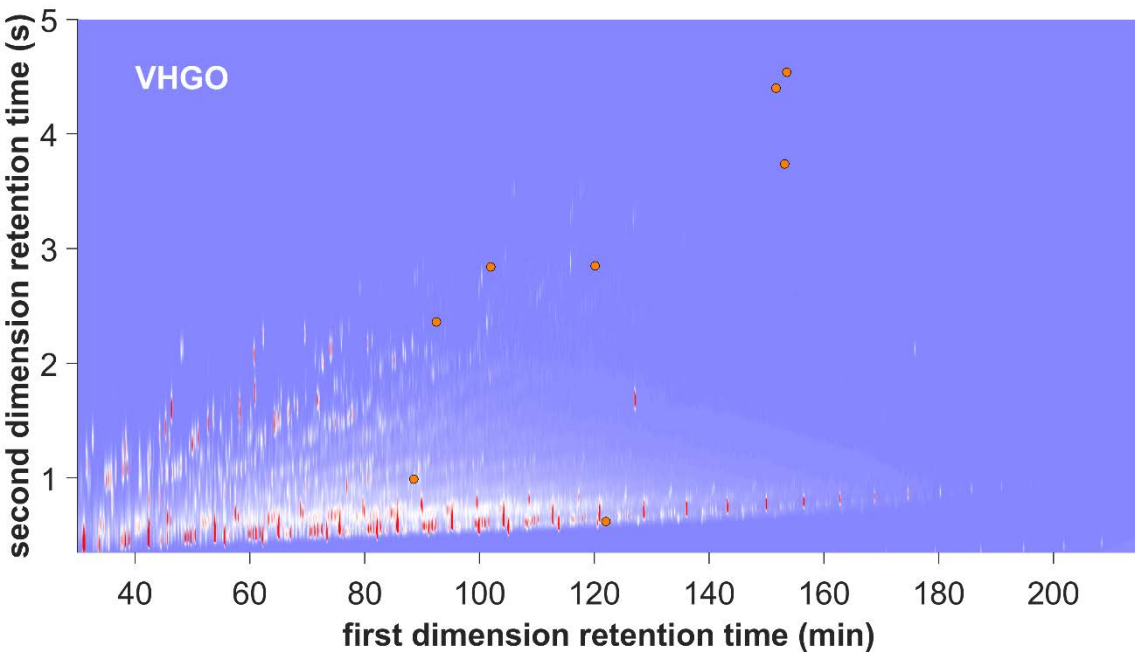

Figure S14. Tracked peaks having DT_{50}s >60 d (filled circles) overlaid on the day-0 chromatogram for VHGO oil.

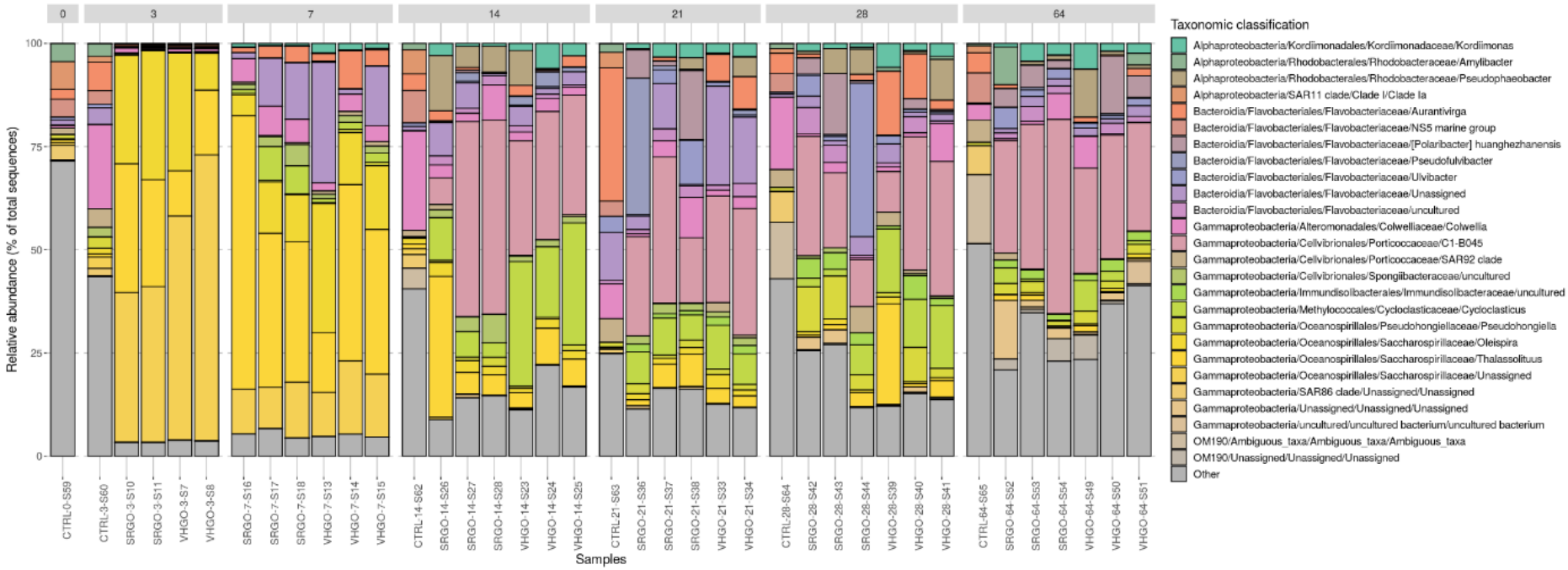

Figure S15. Succession of microbial communities in the VHGO and SRGO, relative to non-oil-containing controls, over the 64 day incubation period.

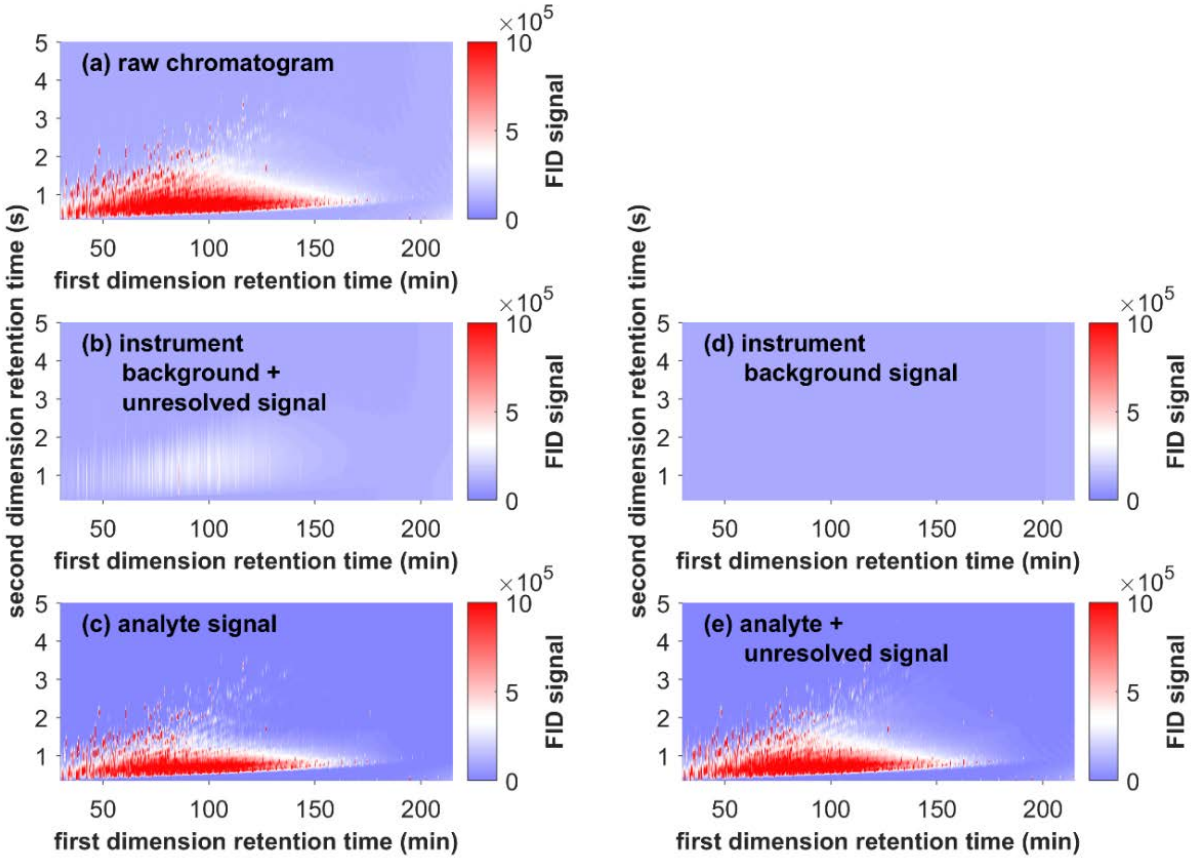

Figure S16. Chromatograms of a raw, non-weathered oil (a) before baseline correction, (b) the combined instrument background and unresolved material baseline calculated with the Eilers algorithm,[8] (c) the non-weathered oil chromatogram after baseline correction with the Eilers algorithm[8] (assumed to correspond to analyte signal, used for quantification of individual peaks). For comparison, (d) shows the instrument background baseline calculated with the Reichenbach et al.[14] algorithm, while (e) is the chromatogram after baseline correction with the Reichenbach et al.[14] algorithm (assumed to correspond to analyte + unresolved signal, used for quantification of total mass of petroleum substance). The color bars are in FID signal units. The terminology used in this figure follows that defined by Samanipour et al.[1]

Figure S17. Remaining mass fraction after evaporative loss based on deuterated PAH peak ratios (open circles, Eq. 2.) and fitted exponential curve used for chromatogram and peak table correction for evaporative losses (solid lines, Eq. 1.). Sample numbers (as defined in Table S4) are written on the individual panels.

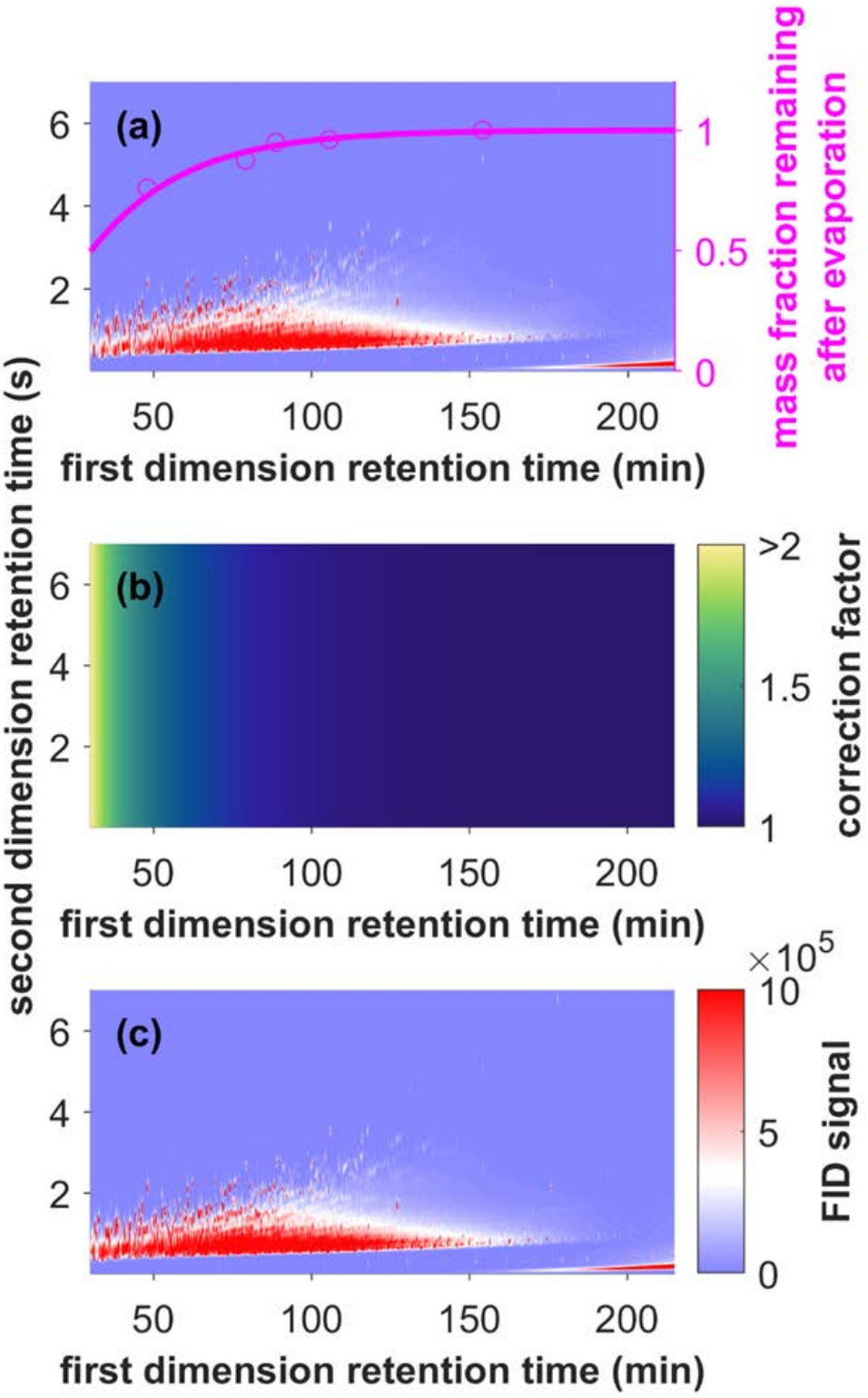

Figure S18. Conceptual depiction of the evaporation correction procedure. (a) Example GC×GC–FID chromatogram before correction for evaporative losses. The chromatogram is overlaid with the observed fraction of mass remaining after evaporation for each of the deuterated PAH internal standards ($F_{remaining}$ in Eq. 2, pink open circles, right y-axis) and the fitted fraction of mass remaining after evaporation ($f_{remaining}$ in Eq. 1, pink solid line, right y-axis). (b) Example of the chromatographic

correction factor for evaporative losses (equal to one divided by $f_{remaining}$ depicted on panel a). (c) Example chromatogram after correction for the evaporative losses.

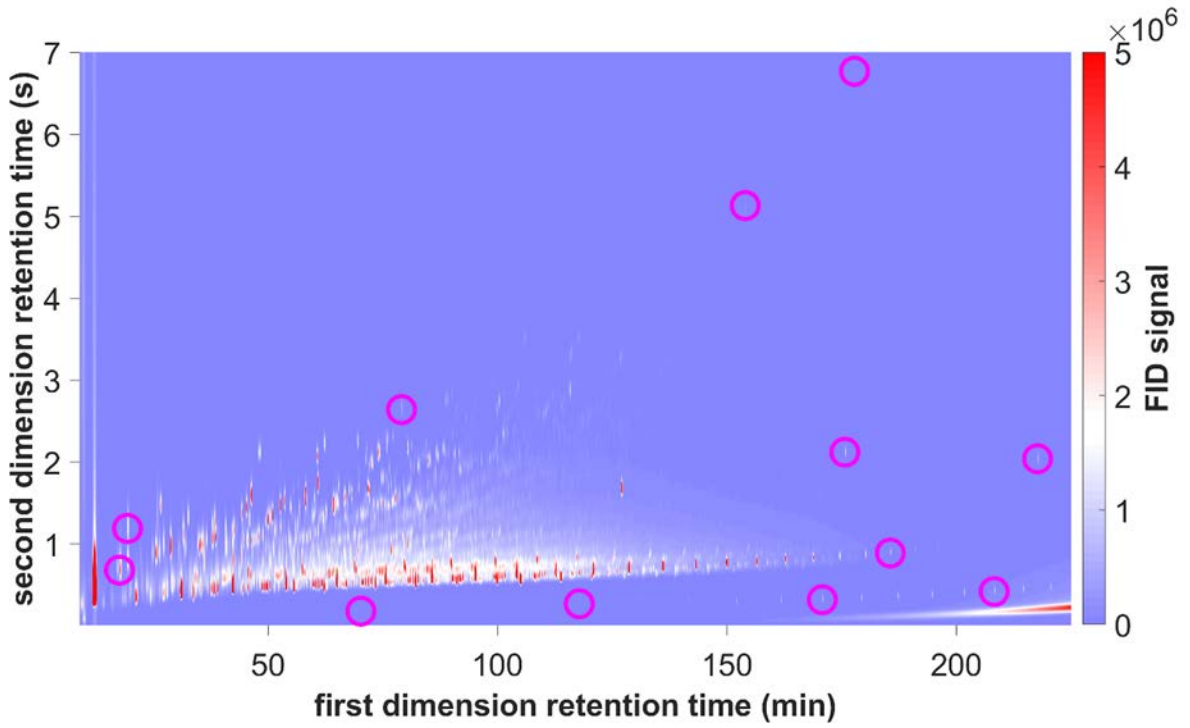

Figure S19. Set of selected alignment points (pink open circles) overlaid on a day-0 chromatogram. The color bar corresponds to "FID signal units", after baseline correction.

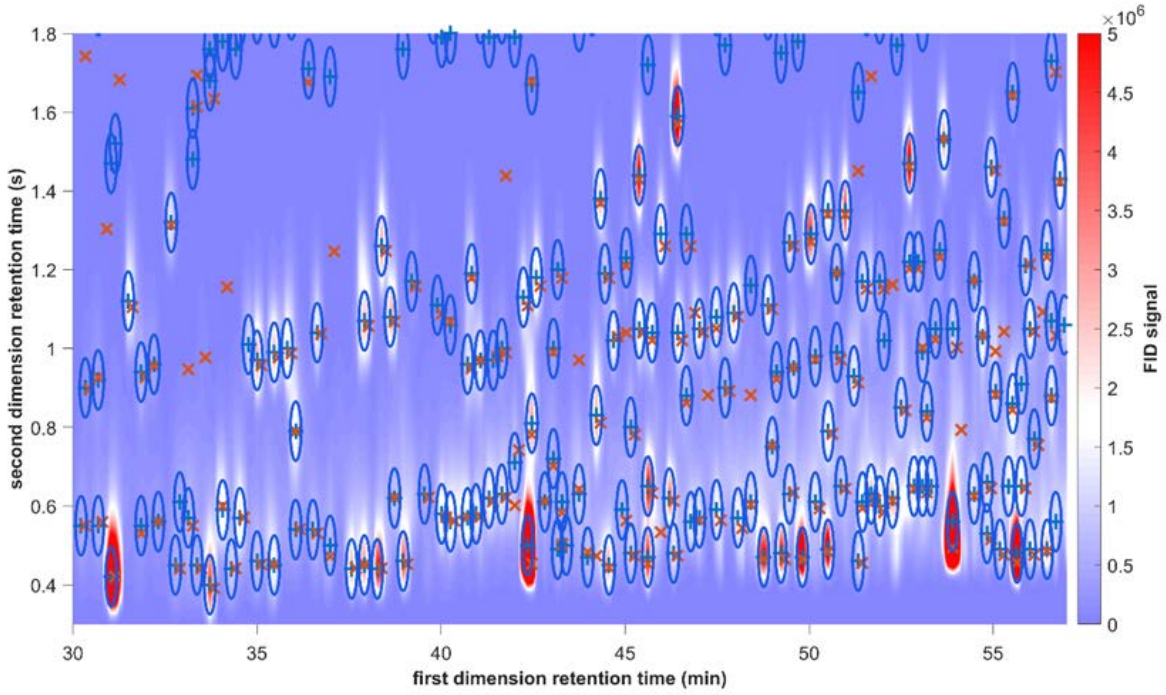

Figure S20. Depiction of the template peaks (blue pluses, here depicted for an example day-0 chromatogram), target peaks (red crosses, here depicted for an example day-7 chromatogram), and search ovals for the template peaks (blue ovals), overlaid on a subset of the day-0 GC×GC–FID chromatogram. Note the good peak separation favored by the long separation time along the first dimension (>200 min for the full chromatogram).

References

(1) Samanipour, S.; Dimitriou-Christidis, P.; Gros, J.; Grange, A.; Samuel Arey, J. Analyte quantification with comprehensive two-dimensional gas chromatography: Assessment of methods for baseline correction, peak delineation, and matrix effect elimination for real samples. *Journal of Chromatography A* **2015**, *1375*, 123-139. DOI: https://doi.org/10.1016/j.chroma.2014.11.049.
(2) Frysinger, G. S.; Gaines, R. B.; Xu, L.; Reddy, C. M. Resolving the Unresolved Complex Mixture in Petroleum-Contaminated Sediments. *Environmental Science & Technology* **2003**, *37* (8), 1653-1662. DOI: 10.1021/es020742n.
(3) Reddy, C. M.; Eglinton, T. I.; Hounshell, A.; White, H. K.; Xu, L.; Gaines, R. B.; Frysinger, G. S. The West Falmouth oil spill after thirty years: The persistence of petroleum hydrocarbons in marsh sediments. *Environmental Science & Technology* **2002**, *36* (22), 4754-4760. DOI: 10.1021/es020656n.
(4) Gros, J.; Reddy, C. M.; Aeppli, C.; Nelson, R. K.; Carmichael, C. A.; Arey, J. S. Resolving biodegradation patterns of persistent saturated hydrocarbons in weathered oil samples from the Deepwater Horizon disaster. *Environmental Science & Technology* **2014**, *48* (3), 1628-1637. DOI: 10.1021/es4042836.
(5) Scarlett, A.; Galloway, T. S.; Rowland, S. J. Chronic toxicity of unresolved complex mixtures (UCM) of hydrocarbons in marine sediments. *Journal of Soils and Sediments* **2007**, *7* (4), 200-206. DOI: 10.1065/jss2007.06.232.
(6) Rowland, S.; Donkin, P.; Smith, E.; Wraige, E. Aromatic Hydrocarbon "Humps" in the Marine Environment: Unrecognized Toxins? *Environmental Science & Technology* **2001**, *35* (13), 2640-2644. DOI: 10.1021/es0018264.
(7) Ventura, G. T.; Kenig, F.; Reddy, C. M.; Frysinger, G. S.; Nelson, R. K.; Mooy, B. V.; Gaines, R. B. Analysis of unresolved complex mixtures of hydrocarbons extracted from Late Archean sediments by comprehensive two-dimensional gas chromatography (GC×GC). *Organic Geochemistry* **2008**, *39* (7), 846-867. DOI: https://doi.org/10.1016/j.orggeochem.2008.03.006.
(8) Eilers, P. H. C. Parametric time warping. *Analytical Chemistry* **2004**, *76* (2), 404-411. DOI: 10.1021/ac034800e.
(9) *Gros-Eilers-Arey code to perform baseline correction of GC×GC chromatograms*; GitHub: GitHub, 2015 https://github.com/jsarey/GCxGC-baseline-correction. https://github.com/jsarey/GCxGC-baseline-correction (accessed.
(10) Gros, J.; Nabi, D.; Dimitriou-Christidis, P.; Rutler, R.; Arey, J. S. Robust algorithm for aligning two-dimensional chromatograms. *Analytical Chemistry* **2012**, *84* (21), 9033-9040. DOI: 10.1021/ac301367s.
(11) Gros, J.; Nabi, D.; Würz, B.; Wick, L. Y.; Brussaard, C. P. D.; Huisman, J.; van der Meer, J. R.; Reddy, C. M.; Arey, J. S. First Day of an Oil Spill on the Open Sea: Early Mass Transfers of Hydrocarbons to Air and Water. *Environmental Science & Technology* **2014**, *48* (16), 9400-9411. DOI: 10.1021/es502437e.
(12) Swarthout, R. F.; Gros, J.; Arey, J. S.; Nelson, R. K.; Valentine, D. L.; Reddy, C. M. Comprehensive two-dimensional gas chromatography to assess petroleum product weathering. In *Hydrocarbon and Lipid Microbiology Protocols: Petroleum, Hydrocarbon and Lipid Analysis*, McGenity, T. J., Timmis, K. N., Nogales, B. Eds.; Springer Berlin Heidelberg, 2017; pp 129-149.
(13) Gros, J. Investigating the fate of petroleum fluids released in the marine environment with comprehensive two-dimensional gas chromatography and transport models. PhD, EPFL, Lausanne, Switzerland, 2016. http://dx.doi.org/10.5075/epfl-thesis-6883.
(14) Reichenbach, S. E.; Ni, M.; Zhang, D.; Ledford, E. B. Image background removal in comprehensive two-dimensional gas chromatography. *Journal of Chromatography A* **2003**, *985* (1), 47-56. DOI: https://doi.org/10.1016/S0021-9673(02)01498-X.
(15) Reichenbach, S. E.; Ni, M.; Kottapalli, V.; Visvanathan, A. Information technologies for comprehensive two-dimensional gas chromatography. *Chemometrics and Intelligent Laboratory Systems* **2004**, *71* (2), 107-120. DOI: https://doi.org/10.1016/j.chemolab.2003.12.009.

(16) Nabi, D.; Gros, J.; Dimitriou-Christidis, P.; Arey, J. S. Mapping Environmental Partitioning Properties of Nonpolar Complex Mixtures by Use of GC × GC. *Environmental Science & Technology* **2014**, *48* (12), 6814-6826. DOI: 10.1021/es501674p.
(17) Arey, J. S.; Nelson, R. K.; Xu, L.; Reddy, C. M. Using Comprehensive Two-Dimensional Gas Chromatography Retention Indices To Estimate Environmental Partitioning Properties for a Complete Set of Diesel Fuel Hydrocarbons. *Analytical Chemistry* **2005**, *77* (22), 7172-7182. DOI: 10.1021/ac051051n.
(18) Schwarzenbach, R. P.; Gschwend, P. M.; Imboden, D. M. *Environmental Organic Chemistry*; John Wiley & Sons, 2003.
(19) Arey, J. S.; Nelson, R. K.; Reddy, C. M. Disentangling oil weathering using GC×GC. 1. Chromatogram analysis. *Environmental Science & Technology* **2007**, *41* (16), 5738-5746. DOI: 10.1021/es070005x.
(20) Arey, J. S.; Nelson, R. K.; Plata, D. L.; Reddy, C. M. Disentangling Oil Weathering Using GC×GC. 2. Mass Transfer Calculations. *Environmental Science & Technology* **2007**, *41* (16), 5747-5755. DOI: 10.1021/es070006p.
(21) *Peakfit.m*; MATLAB Central File Exchange: Https://Www.Mathworks.Com/Matlabcentral/Fileexchange/23611-Peakfit-m, 2021. Https://Www.Mathworks.Com/Matlabcentral/Fileexchange/23611-Peakfit-m (accessed.
(22) Wardlaw, G. D.; Arey, J. S.; Reddy, C. M.; Nelson, R. K.; Ventura, G. T.; Valentine, D. L. Disentangling oil weathering at a marine seep using GC×GC: Broad metabolic specificity accompanies subsurface petroleum biodegradation. *Environmental Science & Technology* **2008**, *42* (19), 7166-7173. DOI: 10.1021/es8013908.
(23) Prince, R. C.; Elmendorf, D. L.; Lute, J. R.; Hsu, C. S.; Haith, C. E.; Senius, J. D.; Dechert, G. J.; Douglas, G. S.; Butler, E. L. 17α(H)-21β(H)-hopane as a conserved internal marker for estimating the biodegradation of crude oil. *Environmental Science & Technology* **1994**, *28* (1), 142-145. DOI: 10.1021/es00050a019.
(24) Tong, H. Y.; Karasek, F. W. Flame ionization detector response factors for compound classes in quantitative analysis of complex organic mixtures. *Analytical Chemistry* **1984**, *56* (12), 2124-2128. DOI: 10.1021/ac00276a033.
(25) Aeppli, C.; Nelson, R. K.; Radović, J. R.; Carmichael, C. A.; Valentine, D. L.; Reddy, C. M. Recalcitrance and Degradation of Petroleum Biomarkers upon Abiotic and Biotic Natural Weathering of Deepwater Horizon Oil. *Environmental Science & Technology* **2014**, *48* (12), 6726-6734. DOI: 10.1021/es500825q.
(26) *Gros-Arey code to align GC×GC chromatograms*; GitHub: GitHub, 2015 https://github.com/jsarey/GCxGC-alignment. https://github.com/jsarey/GCxGC-alignment (accessed.
(27) Zushi, Y.; Gros, J.; Tao, Q.; Reichenbach, S. E.; Hashimoto, S.; Arey, J. S. Pixel-by-pixel correction of retention time shifts in chromatograms from comprehensive two-dimensional gas chromatography coupled to high resolution time-of-flight mass spectrometry. *Journal of Chromatography A* **2017**, *1508*, 121-129. DOI: https://doi.org/10.1016/j.chroma.2017.05.065.
(28) *Arey-Gros code to track GC×GC peaks*; GitHub: GitHub, 2021

https://github.com/jonasgros/GCxGC-peak-tracking. https://github.com/jsarey/GCxGC-alignment (accessed.
(29) Davison, A. C.; Hinkley, D. V. *Bootstrap Methods and their Application*; Cambridge University Press, 1997. DOI: DOI: 10.1017/CBO9780511802843.
(30) Jung, K.; Lee, J.; Gupta, V.; Cho, G. Comparison of Bootstrap Confidence Interval Methods for GSCA Using a Monte Carlo Simulation. *Frontiers in Psychology* **2019**, *10*, Original Research. DOI: 10.3389/fpsyg.2019.02215.
(31) Frysinger, G. S.; Gaines, R. B.; Ledford, E. B. Quantitative determination of BTEX and total aromatic compounds in gasoline by comprehensive two-dimensional gas chromatography (GCxGC). *Journal of High Resolution Chromatography* **1999**, *22* (4), 195-200.

(32) Nelson, R. K.; Kile, B. M.; Plata, D. L.; Sylva, S. P.; Xu, L.; Reddy, C. M.; Gaines, R. B.; Frysinger, G. S.; Reichenbach, S. E. Tracking the weathering of an oil spill with comprehensive two-dimensional gas chromatography. *Environmental Forensics* **2006**, *7*, 33-44.
(33) Nizio, K. D.; Mginitie, T. M.; Harynuk, J. J. Comprehensive multidimensional separations for the analysis of petroleum. *Journal of Chromatography A* **2012**, *1255*, 12-23. DOI: https://doi.org/10.1016/j.chroma.2012.01.078.
(34) B. Gaines, R.; S. Frysinger, G.; M. Reddy, C.; K. Nelson, R. 5 - Oil spill source identification by comprehensive two-dimensional gas chromatography (GC × GC). In *Oil Spill Environmental Forensics*, Wang, Z., Stout, S. A. Eds.; Academic Press, 2007; pp 169-XI.
(35) Pierce, K. M.; Wood, L. F.; Wright, B. W.; Synovec, R. E. A Comprehensive Two-Dimensional Retention Time Alignment Algorithm To Enhance Chemometric Analysis of Comprehensive Two-Dimensional Separation Data. *Analytical Chemistry* **2005**, *77* (23), 7735-7743. DOI: 10.1021/ac0511142.
(36) Gaines, R. B.; Frysinger, G. S.; Reddy, C. M.; Nelson, R. K. Oil Spill Source Identification by Comprehensive Two-Dimensional Gas Chromatography (GC×GC). In *Oil Spill Environmental Forensics*, 1st ed.; Wang, Z., Stout, S. A. Eds.; Academic Press, 2007; pp 169-206.
(37) Prosser, C. M.; Redman, A. D.; Prince, R. C.; Paumen, M. L.; Letinski, D. J.; Butler, J. D. Evaluating persistence of petroleum hydrocarbons in aerobic aqueous media. *Chemosphere* **2016**, *155*, 542-549. DOI: https://doi.org/10.1016/j.chemosphere.2016.04.089.
(38) Pilson, M. E. *An Introduction to the Chemistry of the Sea*; cambridge university press, 2012.

Excel worksheet with peak volumes (relative to day 0) of each tracked peak for each of the sampling time points

Supporting_Information_peak volumes